A model framework on atmosphere-snow water vapor exchange and the associated isotope effects at Dome Argus, Antarctica：part I the diurnal changes

~~A model framework on atmosphere-snow water vapor exchange and the associated isotope effects at Dome Argus, Antarctica：part I the diurnal changes~~

Tianming Ma[1,2], Zhuang Jiang[1], Minghu Ding[43,32], Yuansheng Li[54], Wenqian Zhang[43] and Lei Geng[1, 32, 65]

[1] Deep Space Exploration Laboratory/School of Earth and Space Sciences, University of Science and Technology of China, Hefei 230026, China.
[2] College of Marine Technology and Environment, Dalian Ocean University, Dalian 230026, China
[32] State Key Laboratory of Cryospheric Science, Northwest Institute of Eco-Environment and Resources, Chinese Academy of Sciences, Lanzhou 730000, China.
[43] Chinese Academy of Meteorological Sciences, Beijing 100081, China.
[54] Polar Research Institute of China, Shanghai 200136, China.
[65] CAS Center for Excellence in Comparative Planetology, University of Science and Technology of China, Hefei 230026, Anhui, China.

Correspondence to: Lei Geng (genglei@ustc.edu.cn)

Abstract. Ice-core water isotopes contain valuable information on past climate changes. However, such information can be altered by post-depositional processing after snow deposition. Atmosphere-snow water vapor exchange is one of such processes, but its influence remains poorly constrained. Here we constructed a box model to quantify the atmosphere-snow water vapor exchange fluxes and the associated isotope effects at sites with low snow accumulation rate where the effects of atmosphere-snow water vapor exchange are suspected to be large. The model reproduced the observed diurnal variations of $\delta^{18}O$, δD, and d-excess in water vapor at Dome C, East Antarctica. According to the same model framework, we found that under summer clear-sky conditions atmosphere-snow water vapor exchange at Dome A can cause diurnal variations in atmospheric water vapor $\delta^{18}O$ and δD by ~~8.2~~4.75±~~0.3~~2.57 ‰ and ~~54.4~~28.8±~~1.2~~19.06 ‰, with corresponding diurnal variations in surface snow $\delta^{18}O$ and δD by 0.~~11~~80±0.0~~35~~1 ‰ and ~~1~~0.6~~42~~±2.71~~0.01~~ ‰, respectively. The modelled~~modeled~~ results under summer cloudy conditions display similar patterns to those under clear-sky conditions but with smaller magnitudes of diurnal variations. After 24-hour simulation, snow ~~water~~ isotopes were enriched under both cloudy and clear-sky conditions. Under winter conditions at Dome A, the model predicts that more or less depletions in snow $\delta^{18}O$ and δD ~~indicates there are no diurnal cycles in atmospheric and surface snow water isotopes~~ can be caused by atmosphere-snow water vapor exchange in~~, but the model predicts more or less depletions in snow $\delta^{18}O$ and δD in~~ the period of 24-hour simulation, opposite to the results under

带格式的：上标
带格式的：上标
带格式的：非突出显示
带格式的：非突出显示
带格式的：非突出显示
带格式的：非突出显示
带格式的：非突出显示
带格式的：非突出显示
带格式的：非突出显示
带格式的：非突出显示
带格式的：上标

summer conditions. If the modelled~~modeled~~ snow isotope enrichments in summer and depletions in winter represent general situations at Dome C, this likely suggests the atmosphere~~ir~~-snow water vapor exchange tends to enlarge snow ~~water~~ isotope seasonality, but the annual net effect would be small due to the offsetting of effects in summer and winter. This remains to be explored in the future.

1 Introduction

Water stable isotopes ($\delta^{18}O$ and δD) in snow and rain are valuable proxies to inform atmospheric temperatures at the time of precipitation forms (Craig, 1961; Dansgaard, 1964). In Antarctica, the isotopic composition of snowfall, as well as that of surface snow, are found to be correlated with local air temperature (Fujita et al., 2006; Masson-Delmotte et al., 2008; Stenni et al., 2016). These findings permit past temperature reconstructions using ice-core $\delta^{18}O$ and δD records across different time scales (e.g., from millennium to glacial-interglacial) (Petit et al., 1999; EPICA community members, 2004; WAIS Divide project members, 2013). Temperature information at shorter time scales (e.g., seasonal to decadal or longer) is critical for understanding climate variabilities and probing the driving forces, and thus many studies have been focused on high-resolution temperature reconstructions using water isotope profiles (e.g., Stenni et al., 2017). However, there are increasing observations indicating that air temperature and snow/ice-core water isotopes are not always co-varying, especially at decadal or shorter timescales, and the disconnection is particularly obvious at low snow accumulation rate sites such like Vostok, Dome F and Dome C, Antarctica (Hoshina et al., 2014; Ekaykin et al., 2017; Casado et al., 2018). Such observations suggest the changes in snow water isotopes after deposition, which not only inhibits temperature reconstructions at decadal or shorter timescales using ice core $\delta^{18}O$ and/or δD records, but also undermines the reconstructions at longer timescales such as millennium and glacial-interglacial climate changes (Touzeau et al., 2016; Casado et al., 2018; Laepple et al., 2018; Markle & Steig, 2022).

It is well-known that after snow deposition, there is a combination of post-depositional processes that can induce significant changes in water isotopic compositions of snow (Steen-Larsen et al., 2013; Casado et al., 2018; Laepple et al., 2018). Such changes have been demonstrated by gradually weakening coupling the snow isotope-temperature relationships as reflected by surface and buried snow samples (Casado et al., 2018). Atmosphere-snow water vapor exchange is one of such processes but there are only limited observations/modeling studies focusing on this process at the diurnal scale in polar summers (Ritter et al., 2016; Casado et al., 2018; Madsen et al., 2019; Hughes et al., 2021; Wahl et al., 2021; Hu et al., 2022; Wahl et al., 2022). Isotopic effects associated with atmosphere-snow water vapor exchange at longer time scales remain unclear.

Atmosphere-snow water vapor exchange is the water sublimation-vapor deposition cycle occurring at the atmosphere-snow interface. It is driven by near-surface vapor pressure gradients and influenced by temperature, wind speed, and humidity (Neumann et al., 2009; Sokratov & Golubev, 2009; Ritter et al., 2016; Wahl et al., 2021; Wahl et al., 2022). Dansgaard (1973) proposed that the layer-by-layer sublimation of snow and ice will not induce isotopic fractionation, but this was suggested to be invalid by laboratory experiments and field observations that both found sublimation is subject to modify surface snow isotopic compositions under natural conditions (Sokratov & Golubev, 2009; Ebner et al., 2017; Hughes et al., 2021; Wahl et

al., 2021). Moreover, water vapor sublimated from snow can be transferred to the overlying atmosphere where it affects atmospheric water vapor concentration and isotopic composition. On the other hand, the inverse part of the sublimation, i.e., the deposition, can also lead to changes in isotopic composition of surface snow as well as atmospheric water vapor due to preferential deposition of heavy isotopes (e.g., $H_2{}^{18}O$, HDO) (Wahl et al., 2021). Given fluctuations in surface temperature, humidity and other meteorological conditions, the relative degree of sublimation vs. deposition could vary, leading to variations in isotopic compositions of surface snow and atmospheric boundary layer water vapor (Neumann et al., 2009; Sokratov & Golubev, 2009; Ritter et al., 2016; Wahl et al., 2021; Hughes et al., 2021; Wahl et al., 2022). Parallel variations in the isotopic compositions of atmospheric water vapor and surface snow (0.2-1.5 cm depth) have been observed at multiple polar sites (e.g., Dome C, Kohnen station, NEEM, and EastGrip) in summer for short durations (Steen-Larsen et al., 2013; Casado et al., 2016; Casado et al., 2018; Madsen et al., 2019; Bréant et al., 2019), and such co-variations were suggested to be due to the role of atmosphere-snow water vapor exchange.

Given the difficulties in conducting continuously high-resolution observations in the polar regions, a model frame describing the atmosphere-snow water vapor exchange processes and the associated isotope effects would be useful in terms of snow and ice-core water isotope record interpretation across different sites. Such models, if fully resolving the physical mechanisms of the atmosphere-snow water vapor exchange processes with appropriate parameterizations, can be incorporated into snowpack and climate model to thoughtfully assess the effects of atmosphere-snow water vapor exchange on the preservation of snow water isotope signals. Several empirical models have been developed to evaluate the isotope effects of atmosphere-snow water vapor exchange. They incorporates atmospheric stratification and climatological boundary conditions to calculate water mass and isotope exchanges at the snow-air interface by assuming a closed system with a one-dimensional box model. (Ritter et al., 2016; Casado et al., 2018; Pang et al., 2019).

As the interior dome of East Antarctica, Dome Argus (80.42°S, 77.12°E; 4093 m above sea level, Dome A hereafter) has a more southerly moisture source compared to other sites in the East Antarctic Plateau (Wang et al., 2012). This makes ice core records of water isotopes from Dome A special in terms of recording southern mid-altitude moisture influence. In addition, Dome A is a candidate site in search of ancient ice with 1-1.5 million years old (Sun et al., 2008; Van Liefferinge et al., 2018). Since 2009, the Kunlun deep ice coring project was conducted at Dome A. By the field season of 2015/2016, an 800-m ice core has been drilled (Hu et al., 2021), and preliminary analysis on water isotopic records of the top 109 meters reflects a long-term cooling trend at Dome A in the last 2 kyr (Hou et al., 2012; Jiang et al., 2012; An et al., 2021). Given the extremely low snow accumulation rate (18-23 mm w. eq. y., Ding et al., 2016) at Dome A, water isotopes preserved in firn and ice cores at this site are presumably influenced by post-depositional processing, especially the effects of atmosphere-snow water vapor exchange might become important as snow can stay at the surface for a relatively long period given the low snow accumulation rate. This characteristic not only means water isotope records from Dome A should be carefully evaluated for the effects of atmosphere-snow water vapor exchange before interpretation, but also makes Dome A a promising site to elucidate the isotopic effects of atmosphere-snow water vapor exchange. In addition, reanalysis data indicate that at Dome A the time interval between two precipitation events can be as long as ~ 80 days, which means snow can sit at the surface for a substantially long

period before burial, subject to experiencing extensive atmosphere-snow water vapor exchange with consequences on isotopic compositions of the buried snow. Pang et al. (2019) has estimated the potential influence of summer (November to January) sublimation on isotopic composition of surface snow at Dome A using a simple Rayleigh distillation model. They found on average surface snow $\delta^{18}O$ was enriched by 1.99 ‰ compared to fresh snow $\delta^{18}O$. However, this evaluation may underestimate the isotopic effects since it did not consider potential effects of e.g., atmospheric dynamical conditions and cloud. A new model is thus needed to provide a more comprehensive evaluation on the isotopic effect of ~~snow-a~~tmosphere-snow water~~ir~~ vapor exchange at Dome A, especially for seasons other than summer months when observations are not available.

To provide a more comprehensive assessment on the effects of atmosphere-snow water vapor exchange for snow and atmospheric water isotope variations at Dome A, we constructed an improved one-dimensional box model based on previous work (Ritter et al., 2016; Touzeau et al., 2018) to predict changes in snow and water vapor isotopic compositions at Dome A within diurnal scale. The main characteristics compared to models in the literature includes the use of bulk aerodynamic method to parameterize atmosphere-snow water vapor exchange. This model was first validated by observations at Dome C and then applied under Dome A conditions.

2 Method

2.1 Model construction and description

~~Similar to~~Similar to the model developed by ~~Ritter et al. (2016)~~Casado et al., (2018), the model presented in this study contains three~~wo~~ water reservoirs, i.e., the free atmospheric water vapor layer, ~~near-surface~~the atmospheric boundary ~~atmospheric water vapor~~ layer and the topmost snow layer (Fig. 1). Their masses and isotopic compositions are considered to be only associated with two processes, i.e., atmosphere-snow water vapor exchange occurring at the atmosphere-snow interface and the advection of air masses occurring between the free atmospheric and boundary layers. ~~For~~ These two processes can cause changes in the masses and isotopic compositions of water vapor in the boundary layer, whereas t~~both reservoirs, he~~~~their~~ masses and isotopic compositions of snow layer are ~~assumed to be~~ only ~~affected~~ influenced by atmosphere-snow water vapor exchange ~~in vertical orientations~~.

The atmosphere-snow water vapor exchange is consisted of two processes, i.e., sublimation and deposition (Fig. 1). During sublimation, water vapor is released from snow, transported into the atmospheric layer via turbulent mixing and molecular diffusion, and immediately mixed with the water vapor already in the ~~near-surface atmospheric~~boundary layer. During deposition, water vapor is influenced by aerodynamic resistance from turbulence and molecular diffusion, and the deposit is mixed with the surface snow layer ~~followed by a mixing procedure and then uptake of surface snow~~. While water vapor transportation at the atmosphere-snow ~~water~~ interface relies on two different diffusion pathways, turbulence plays a more crucial role in the mass and energy exchanges (Brun et al., 2011; Vignon et al., 2017).

In the box model, atmosphere-snow water vapor exchange flux is calculated by turbulent quantities at each time step of 1 hour, as detailed in Section 2.1.1. Based on atmosphere-snow water vapor exchange flux parameterization, the model further

带格式的：非突出显示
带格式的：非突出显示
带格式的：非突出显示

calculates temporal variations in snow and water vapor isotopic compositions according to isotopic mass balance (detailed in Section 2.1.2).

Model inputs mainly include meteorological conditions, e.g., air temperature (T_a), surface temperature (T_s), humidity (relative humidity (RH_w) or specific humidity (q_a)), and wind speed (u_{az}), ~~etc~~. Additional model inputs are mixing-layer height (H_0), snow layer thickness (h_0), as well as the initial isotopic values, ~~(~~i.e., snow isotopic composition (δ_{s0}), ~~and~~ water vapor isotopic composition in the boundary layer (δ_{v0}), and water vapor isotopic composition in the advected air mass (δ_{f0})~~)~~.

2.1.1 Atmosphere-snow water vapor exchange flux parametrization

We used the bulk aerodynamic method and Monin-Obukhov similarity theory (Monin & Obukhov, 1954) to estimate turbulent fluxes. This approach calculates the net effects of sublimation and deposition at each time step using meteorological data, avoiding to parameterize the individual fluxes of sublimation and deposition.

The bulk aerodynamic method estimates atmosphere-snow water vapor exchange flux (Ex~~x~~) through calculation of latent heat (LE) between the surface and one reference height (z) in the boundary layer~~atmospheric level (4 m)~~ (Berkowicz & Prahm, 1982). The expression is as follows:

$$Ex = \frac{LE}{L_s} = LE/Ls = -\rho_a u^* q^* \rho_a \times L_s/r_a \times ((q_s - q_a) + \frac{dq_a}{dt} \times \frac{dT}{dt}) \quad (1)$$

where ρ_a is dry air density varying with observed air temperature (T_{aa}) and pressure (P_{aa}), L_s is sublimation heat constant, u^* and q^* are the friction velocity and specific humidity turbulent scale, respectively. Where u^* and q^* are defined as:

$$u^* = \frac{ku_a}{log(\frac{z}{z_0}) - \Psi_M(\frac{z}{L})} \quad (2)$$

$$q^* = \frac{k(q_a - q_0)}{log(\frac{z}{z_0}) - \Psi_M(\frac{z}{L})} \quad (3)$$

where k denotes the von-karman constant, ~~L_s is sublimation heat constant,~~ u_a is wind speed ~~at~~ the reference height in the boundary layer ($z = 4$m), q_0 is the saturated specific humidity at the snow surface derived from the Clapeyon-Clausius equation, q_a is the specific humidity that can be estimated from observed relative humidity over ice surface (RH_i) once the saturated specific humidity at the reference height (q_a) is known from the Clapeyon-Clausius equation at a given temperature (T_a). z_0 represents surface roughness length for humidity exchange, Ψ_M is diabatic correction term with respect to the ratio of the reference layer height (z) and Monin-Obukhov length (L), where~~r_a is aerodynamic resistance from a reference height (z) in the boundary layer to snow surface, q_s is the saturated specific humidity over ice surface derived from Clapeyon-Clausius equation, q_a is the specific humidity that can be estimated from relative humidity over ice (RH_i) once q_s is known, and the term dqa/dt×dT/dt is the time derivatives of specific humidity and air temperature.~~

带格式的：下标
带格式的：下标
带格式的：非突出显示
带格式的：字体：倾斜
带格式的：字体：倾斜，突出显示
带格式的：字体：倾斜
带格式的：字体：倾斜
带格式的：字体：倾斜
带格式的：字体：倾斜
带格式的：字体：倾斜
带格式的：字体：倾斜
带格式的：字体：倾斜
带格式的：字体：倾斜
带格式的：字体：倾斜
带格式的：字体：倾斜，下标
带格式的：字体：倾斜
带格式的：字体：倾斜
带格式的：字体：倾斜
带格式的：字体：倾斜
带格式的：字体：倾斜，下标
带格式的：字体：非倾斜
带格式的：字体：倾斜，非突出显示
带格式的：非突出显示
带格式的：字体：倾斜

~~The aerodynamic resistance r_a in Eq. (1) is calculated according to Monin-Obukhov similarity theory (Monin & Obukhov 1954), given by transfer coefficient for humidity (C_E) and wind speed (u_z) as follows:~~

~~$r_a = \frac{1}{C_E \times u_z}$ (2)~~

~~The C_E can be expressed as:~~

~~$C_E = \left(\frac{k}{log\left(\frac{z}{z_0}\right) - \Psi_M\left(\frac{z}{L}\right)}\right)^2$ (3)~~

~~where k denotes the von-karman constant, z_0 represents surface roughness length for humidity exchange, Ψ_M is diabatic correction term with respect to the ratio of the reference layer height (z) and Monin-Obukhov length (L). Where~~ L is defined as:

$$L = \frac{\overline{\theta}}{g}\frac{u_*^2}{k\theta_*} \quad (4)$$

where $\overline{\theta}$ is the mean potential temperature between snow surface (θ_0) and the reference height in the boundary layer (θ_{az}), g is the gravity acceleration, u^* and θ^* are friction velocity and temperature turbulent scale, respectively. Where ~~u^* are given by u_z, z_0, and z/L as follows:~~

~~$u_* = \frac{ku_z}{log\left(\frac{z}{z_0}\right) - \Psi_M\left(\frac{z}{L}\right)}$ (5)~~

~~and~~ θ^* is analogous to u^* and q^*, using θ_{az}, z_0, and z/L:

~~$\theta^* = \theta_*$~~ $= \frac{k(\theta_{az} - \theta_0)}{log\left(\frac{z}{z_0}\right) - \Psi_M\left(\frac{z}{L}\right)}$ (6)

In~~From~~ Eq~~:s~~ (2), Eq : (3), and~~-~~ Eq : (5)~~(6)~~, ~~C_E can be determined if z_0 and Ψ_M are known. Here~~ z_0 can be estimated using least square fitting with observed wind speed at three different heights in the neutral atmospheric stratification. The Ψ_M is calculated for stable, unstable and neutral boundary layer using the functions taken from Holtslag & De Bruin (1988). Note that both z_0 and Ψ_M are associated with atmospheric stability. The judgement of atmospheric stability depends on the Richardson number (Ri), which is defined as follows:

~~R_i~~$Ri = \frac{g}{\theta_z} \times \frac{z\Delta\theta}{u_z^2}$ (7)

Based on Eqs: (1)-(67), the atmosphere-snow water vapor exchange flux, Ex, can be calculated in the model with appropriate inputs. A positive value of Ex represents net sublimation (i.e., sublimation > deposition), while a negative value of Ex corresponds to net deposition (i.e., sublimation < deposition).

2.1.2 Isotopic Mass Balance

Assuming that the ~~mass balance between the~~ snow~~two~~ reservoir~~s~~ is only influenced by atmosphere-snow water vapor exchange (Fig. 1), temporal variations in ~~water vapor and~~ snow mass per unit surface area (S) can be expressed as:

~~$M_s^t Ex = M_s^{t-1-1} - Ex - M_s^t = M_{si}^t - M_{si}^{t-1}$~~

(78)

带格式的：字体: 倾斜
带格式的：下标
带格式的：字体: 倾斜
带格式的：字体: 倾斜
带格式的：字体: 倾斜
带格式的：字体: 倾斜
带格式的：字体: 倾斜
带格式的：字体: 倾斜
带格式的：字体: 倾斜
带格式的：字体: 倾斜
带格式的：字体: 倾斜
带格式的：字体: 倾斜
带格式的：下标
带格式的：字体: 倾斜
带格式的：字体: 倾斜
带格式的：字体: 倾斜
带格式的：字体: 倾斜
带格式的：非上标/ 下标
带格式的：字体: 倾斜
带格式的：字体: 倾斜, 非上标/ 下标
带格式的：字体: 倾斜
带格式的：字体: 倾斜, 非上标/ 下标
带格式的：字体: 倾斜
带格式的：字体: 倾斜, 非上标/ 下标

where ~~Ex E_x~~ is the exchange flux as calculated in the previous section, M_s is the mass of the defined surface snow, the superscript of t denotes the time. From Eq: (7), M_s at time t can be calculated from the initial snow masses (i.e., masses at t=0) and the accumulated E_x by time t. In the model, M_s at t=0 relies on initial snow height (h_0) and snow density (ρ_s). For the water vapor mass in the boundary layer (M_v) at time t, it can be computed from initial boundary height (H_0), dry air density (ρ_a), and the specific humidity (q_a) at the reference height in the boundary layer:

$$M_v^t = \rho_a H_0 q_a^t S \quad (8)$$

~~whereas~~where q_a at time t can be determined by direct measurements or the observed relative humidity (RH_a). In Eq: (8), we neglect the temporal changes in the height of the boundary layer, given that the boundary height in polar inland regions are relatively stable (Bonner et al., 2009; Ma B. et al., 2020). From Eq: (8), the mass changes of atmospheric boundary water vapor layer at each time interval is $\rho_v H_0(q_a^t - q_a^{t-1})$. This quantity is influenced by atmosphere-snow water vapor exchange (E_x) and the water vapor advection flux from free atmosphere to the boundary atmospheric layer (M_f). Thus, the M_f at any time can be quantified as follows:

$$M_f^t = M_v^t - M_v^{t-1} - Ex = \rho_v H_0(q_a^t - q_a^{t-1}) - Ex \quad (9)$$

Note the advection between the boundary layer and the free atmosphere can happen under the unstable conditions or some weak stable conditions (Zilitinkevich et al., 2008). In the model, we consider M_f can contribute to the atmospheric boundary water vapor reservoir when the Richardson number is below 0.1 (i.e., including weak stable conditions in addition to unstable conditions).

Based on the calculation of mass changes in the three reservoirs (Eq: (7-9)), ~~M_v is the water vapor mass in the near-surface atmospheric layer, the superscript of t denotes the time. From Eq: (8), M_s and M_v at time t can be calculated from the initial snow and vapor masses (i.e., masses at t=0) and the accumulated E_x by time t. In the model, M_s at t=0 relies on initial snow height (h_0) and snow density (ρ_s), whereas M_v at t=0 is computed from initial near-surface boundary height (H_0), dry air density (ρ_v), and specific humidity (RH_t).~~

t~~T~~he isotopic mass equation~~s~~ ~~are~~:

~~$M_v^{t+1}R_v^{t+1} = M_v^t R_v^t + R_{Ex}^t \times Ex$ (9.a)~~

$M_s^{t+1}R_s^{t+1} = M_s^{t-1}R_s^{t-1} - R_{Ex}^t \times Ex$ (~~9.b~~10.a)

$M_v^t R_v^t = M_v^{t-1}R_v^{t-1} + R_{Ex}^t \times Ex + R_f^t \times M_f^t$ (10.b)

where R_v, ~~R_s~~, R_v, R_f, and R_{Ex} ~~R_s, and R_{Ex}~~ represent the ratios of heavy isotopes (^{18}O and D) and light isotopes (^{16}O and H) ~~in near surface atmospheric water vapor reservoir,~~ in the snow layer~~,~~ ~~and the~~ atmospheric boundary layer, free atmospheric layer, and exchange flux, respectively. ~~In Eq: (9.a) and (9.b), R can also be replaced by the related δ values ($\delta = (R/R_{vsmow} - 1) \times 1000$).~~

The calculation of R_{Ex} is different between sublimation-dominated (i.e., net sublimation) period and deposition-dominated (i.e., net deposition) period. For the sublimation-dominated phase (E_x>0), kinetic fractionation is assumed to occur when sub-saturation condition is taken into account. Isotopic composition of the sublimated vapor is calculated from Merlivat & Jouzel

带格式的: 字体: 倾斜
带格式的: 字体: 倾斜
带格式的: 字体: 倾斜
带格式的: 字体: 倾斜
带格式的: 字体: 倾斜
带格式的: 字体: 倾斜
带格式的: 字体: 倾斜
带格式的: 字体: 倾斜
带格式的: 字体: (中文) +中文正文 (宋体), (中文) 中文(中国)
带格式的: 左
带格式的: 字体: 倾斜
带格式的: 非突出显示
带格式的: 下标
带格式的: 非突出显示
带格式的: 下标
带格式的: 字体: 倾斜
带格式的: 字体: 倾斜
带格式的: 字体: (中文) Times New Roman
带格式的: 字体: (中文) +中文正文 (宋体), (中文) 中文(中国)
带格式的: 字体: 倾斜
带格式的: 字体: 倾斜, 下标
带格式的: 字体: 倾斜
带格式的: 字体: 倾斜
带格式的: 字体: 倾斜, 下标
带格式的: 字体: 倾斜
带格式的: 字体: 倾斜

(1979), combining with R_s, R_v, diffusion coefficient (k'), equilibrium coefficient (α_e), ~~and~~ the relative humidity of the air with respect to the surface temperature (h) ~~the relative humidity (RH_i)~~ as follows:

$$R_{Ex}^t = \frac{1-k'}{1-h\,RH_i}\left(\frac{R_s^t}{\alpha_e} - RH_i h \times R_v^t\right) \quad (10)$$

Isotopic composition of condensed vapor (E_x<0) is in equilibrium with bulk of vapor above -20°C. However, kinetic fractionation will also occur due to vapor supersaturation over ice on the East Antarctic plateau. This effect can reduce the effective fractionation of water isotopes. Given that, the equilibrium coefficient (α_e) is replaced by the effective fractionation coefficient (α_f) when calculating R_{Ex} of condensed vapor. The α_f is defined by the product of the kinetic fractionation coefficient (α_k) and α_e. R_{Ex} of condensed vapor is thus expressed as:

$$R_{Ex}^t = \alpha_f(R_v^t + 1) - 1 \quad (11)$$

The α_e with respect to ice is given by Ellehoj et al. (2013) as a function of temperature (Eq: (13)~~2~~).

~~$\alpha_e^D = exp(0.2133 - \frac{203.10}{T} + \frac{48888}{T^2})$ (12.a)~~

$$\alpha_e^{18O} = exp(0.0831 - \frac{49.192}{T} + \frac{8312.5}{T^2}) \quad (12.ab)$$

$$\alpha_e^{D} = exp(0.2133 - \frac{203.10}{T} + \frac{48888}{T^2}) \quad (13.b)$$

The α_f is deduced from α_e as following:

$$\alpha_f = \alpha_e \frac{RH_i}{1+\alpha_e(RH_i-1)(\frac{D_i}{D_i'})} \quad (13)$$

where D_i is the diffusivity of water molecule and D_i' denotes the same as D_i but for heavy isotopes. The ratios of D_i / D_i' is given by Jouzel & Merlivat (1984), with a value of 1.0285 for ^{18}O and 1.0251 for D.

Key variables in the model are summarized and listed in Table S1.

2.2 Model simulations

We first used the above-mentioned model to simulate atmosphere-snow water vapor exchange and the associated isotope effects at Dome C (75.10°S, 123.33°E; 3233 meters above sea level) where diurnal variations in water vapor isotopic compositions as well as surface snow water isotopes are available from observations (Casado et al., 2016; Touzeau ~~Casado~~ et al., 2016). We then applied the model to Dome A conditions to investigate the isotopic effects due to atmosphere-snow water vapor exchange at diurnal scales. Model initial values including mixing-layer height (H_0), snow layer height (h_0), snow isotopic composition (δs_0), water vapor isotopic composition in the boundary layer (δv_0), water vapor isotopic composition in the advected air mass (δf_0), and ~~and~~ snow density (ρ_s) are listed in Table 1. These values were justified according to conditions as discussed in the following sections.

带格式的: 字体: 倾斜
带格式的: 字体: 倾斜
带格式的: 非突出显示
带格式的: 非突出显示
带格式的: 非突出显示
带格式的: 非突出显示
带格式的: 字体: 倾斜
带格式的: 字体: 倾斜
带格式的: 字体: 倾斜
带格式的: 字体: 倾斜
带格式的: 非突出显示
带格式的: 字体: 倾斜
带格式的: 字体: 倾斜
带格式的: 字体: 倾斜
带格式的: 字体: 倾斜
带格式的: 字体: 倾斜
带格式的: 非突出显示
带格式的: 字体: 10 磅, 非倾斜
带格式的: 非突出显示

2.2.1 Diurnal simulations under Dome C conditions

At Dome C, previous observations have found a clear diurnal cycle of water vapor isotopic composition from 5 to 16 January 2015 (Casado et al., 2016). This diurnal cycle was attributed to the effects of atmosphere-snow water vapor exchange in a stable atmospheric boundary layer under clear-sky conditions over ~~the~~ an ~~period~~ 11 days of observations (~~11 days~~Casado et al., 2018). ~~Based on these observations, we produced a representative diurnal cycle of isotopes with uncertainties by stacking the 11 observed cycles.~~ To compare modelled results with observations, we performed the continuous simulation over the same period (11 days) using observed meteorological data over this period (The results can be seen in text S3 of SI). Meteorological parameters (e.g., temperature, humidity, and wind speed~~, etc.~~) over the period of observation were downloaded from the CALVA program (Genthon et al., 2010). The surface snow temperature (T_s) was available in the previous publication (Casado et al., 2016)~~, calculated based on the method from Brun et al. (2011). The equation for T_s calculations is shown as follows:~~

~~$$T_S = \left(\frac{LW_{up}+(\epsilon-1)LW_{dn}}{\epsilon\sigma}\right)^{0.25} \quad (14)$$~~

~~where σ is the Stefan–Boltzmann constant, ϵ is the snow emissivity (0.93), LW_{dn} and LW_{up} are the downward and upward longwave radiative fluxes respectively. The hourly data for longwave radiative fluxes were retrieved from ERA5 reanalysis dataset. In order to better compare with the observed isotopes values, we also stacked the 11 days meteorological data to produce representative diurnal cycles of temperature, humidity, wind speed and etc.~~

The boundary height, H_0, was determined by Doppler Sodar measurements from an on-site iron tower at Dome C (Vignon et al., 2017). The surface snow layer height, h_0, was set to be the thickness of surface snow collected (i.e., 1.5 cm) for isotopic composition analysis at this site (Casado et al., 2018). ~~The density of surface snow, ρ_s, was reported by Laepple et al. (2018).~~ The initial ~~atmospheric~~ vapor isotopic compositions in the boundary layer, δv_0, were~~ere~~ set as the ~~11-day averages~~ observations of~~of~~ water vapor $\delta^{18}O$, δD, and d-excess at the beginning of modelling period~~at 00:00 UTC from observations~~ during the 2014/2015 field season (Casado et al., 2016), while snow isotopes, δs_0, were set as the mean isotopic values of ~~surface~~ precipitated snow samples ~~collected from campaign NIVO during 2013-2016~~ (Casado et al., 2018). The isotopic composition of advected air masses (δf_0) was not observed at this site. However, considering that advection occurs under warm air masses, it can be relatively positive with respect to δv_0, as noted by Casado et al. (2018). The δf_0 was thus set to be the highest observed value of water vapor $\delta^{18}O$ and δD at Dome C. The density of the topmost 5 cm of the surface snow (ρ_s) was reported by Champollion et al. (2019)~~The density of surface snow, ρ_s, was reported by Laepple et al. (2018).~~

2.2.2 Diurnal simulations under Dome A conditions

Previous observations found that a diurnal cycle is clearly shown in surface snow and water vapor isotopic compositions during clear-sky days, whereas this feature is not significant during highly cloudy period (Casado et al., 2016; Ritter et al., 2016; Hughes et al., 2021). Clouds play an important role in modulating atmospheric thermal and dynamic conditions (Haynes et al., 2013), and cloudy conditions may also mean more moisture present in the atmosphere. It is probably under cloudy conditions

带格式的: 字体: 10 磅, 非倾斜
带格式的: 非突出显示
带格式的: 非突出显示
带格式的: 字体: 倾斜
带格式的: 字体: 倾斜
带格式的: 字体: 倾斜
带格式的: 字体: 倾斜
带格式的: 下标
带格式的: 字体: 倾斜
带格式的: 字体: 倾斜, 下标
带格式的: 字体: 倾斜
带格式的: 字体: 倾斜, 下标
带格式的: 下标
带格式的: 上标
带格式的: 下标
带格式的: 非上标/ 下标
带格式的: 非上标/ 下标

extra moisture and downward radiation from cloud disturb local temperature and/or humidity variabilities, making smaller differences between the day and night atmosphere-snow water vapor exchange and thus the isotopic effects are less pronounced. Therefore, in the model simulations for Dome A, we simulated two representative cases with and without cloud (i.e., cloudy vs. clear-sky conditions) in order to accurately ~~fully~~ assess the ~~accumulated~~ isotopic variations associated with~~e effects of~~ atmosphere-snow water vapor exchange.

~~Therefore, in the model simulations for Dome A, we simulated two representative cases with and without cloud (i.e., cloudy vs. clear-sky conditions) in order to fully assess the accumulated isotope effects of atmosphere-snow water vapor exchange.~~

The hourly averages of total cloud cover (Tcc) were used to select days showing clear-sky and highly cloudy conditions. They can be retrieved from the ERA-5 reanalysis dataset, with a spatial resolution of 1.25°×1.25°. Based on previous studies, the classification criteria are as follows: $Tcc \leq 0.3$ for clear-sky conditions, $Tcc \geq 0.8$ for highly cloudy conditions (Qian et al., 2012). In accordance with this criterion, we selected 20 clear-sky days during the summer period (December to February) of 2005-2011. Then, the hourly meteorological data from those selected days were stacked to create a representative cycle for model initialization. For highly cloudy conditions, the stack of 102 diurnal cycles of meteorological variables was also produced for the purpose of modelling on the diurnal scale.

Meteorological data were obtained from an automatic weather station (AWS) installed near the summit of Dome A. The hourly surface air pressure, air temperature at 1 m, 2 m and 4 m height, relative humidity at 4 m height, wind speed at 1 m, 2 m and 4 m height, and wind direction are available for the period of 2005-2011 (Ma et al., 2010; Ding et al., 2022). The surface snow temperature (T_s) were not available observations at Dome A. Thus, we performed T_s ~~was calculated using Eq. (14). Then, these meteorological variables were processed and/or calibrated to produce stacked diurnal cycles as model inputs (Supplementary, Text. S1).~~ calculation~~sed~~ based on the method from Brun et al. (2011). The equation for T_s calculations is shown as follows:

$$Ts = \left(\frac{LW_{up}+(\epsilon-1)LW_{dn}}{\epsilon\sigma}\right)^{0.25} \quad (154)$$

where σ is the Stefan–Boltzmann constant, ϵ is the snow emissivity (0.933), LW_{dn} and LW_{up} are the downward and upward longwave radiative fluxes respectively. The hourly data for longwave radiative fluxes were retrieved from ERA5 reanalysis dataset. ~~In order to better compare with the observed isotopes values, we also stacked the 11 days meteorological data to produce representative diurnal cycles of temperature, humidity, wind speed and etc.~~

The stacked hourly mean values of meteorological conditions at Dome A are shown in Fig. 2a. During clear-sky conditions, the air temperature at 4m level (T_a) shows a diurnal cycle with an amplitude of 10.38°C and an average of 31.01°C. T~~t~~he diurnal T_s varies in parallel with ~~*air temperature at 4m level*~~T_a, ranging from -38.69°C to -27.67°C. The ranges of diurnal cycles is 1.8-3.7×10^{-4} kg·kg^{-1} for specific humidity (q_a) and 66-130% for relative humidity (RH_i). The ~~*specific humidity (*~~q_a~~)~~ also has a parallel evolution with T_a ~~air temperature~~, whereas ~~*the relative humidity*~~RH_i shows an opposite trend. Different from temperature and humidity, the daily air pressure near the surface are stable (~584 hPa) on a diurnal scale. T~~T~~he wind speed (u_a) and latent heat flux ~~and calculated latent heat~~ exhibits the daily~~a~~ ~~diurnal cycle~~ maximum of 2.98 m/s and 3.34 W·m^{-2} at

带格式的 ... [1]
带格式的：字体: 倾斜
带格式的 ... [2]
带格式的 ... [3]
带格式的 ... [4]
带格式的 ... [5]

10:00 UTC, respectively. They coincide with the highest T_a, T_s and ρ_a on the same time within a diurnal cycle. ~~like Ts and q.~~ In comparison, under highly cloudy conditions, ~~all meteorological conditions~~the latent heat are less variable but the ρ_a and μ_a shows the larger variations at the diurnal scale (Fig. 2b).

The model initial values of H_0, h_0, δs_0, δv_0, and ρ_s for Dome A simulations are also listed in Table 1. The H_0 was estimated as the median thickness of the boundary layer (15 m) from sonic radar and seeing—the angular size of stellar images during summer (Bonner et al., 2009; Ma B. et al., 2020). The surface snow thickness, h_0, was set to 1.5 cm according to summer snow accumulation at Dome A (calculated from annual mean snow accumulation of 18-23 mm w. eq. y.). This snow thickness was also applied to perform model simulations at Dome C. The δs_0 values were obtained from the averaged measurements of precipitation isotopic composition in the field season of 2009/2010 at Dome A (Pang et al., 2019). The δv_0 can be calculated from δs_0 assuming atmosphere-snow equilibrium and using the equilibrium fractionation coefficient at a surface temperature of the starting of the diurnal cycle. The δf_0 was set to be the same value as those in Dome C, since there are no measurements at Dome A. The ρ_s shown in Table 1 was from the measurements during the field season of 2014/2015 (Ma T. et al., 2020).

2.2.3 Diurnal simulations under Dome A winter conditions

Given the different meteorological conditions in winter compared to summer, the degree of atmosphere~~ir~~-snow water vapor exchange and the associated isotope effects could be different. Therefore we also conducted simulations for winter at Dome A, and this may shed light on assessment of the effects of the atmosphere-snow water vapor exchange~~air-snow vapor exchange~~ on seasonal and annual scales.

The stacked hourly mean values of winter meteorological conditions at Dome A were extracted in the same way as we did for the summer conditions. As shown in Fig. 2c, unlike in summer, the winter data does not show any apparent diurnal variations~~all diurnal meteorological parameters are less variable in winter compared to summer~~. In addition, the average temperature, specific humidity and atmospheric pressure are lower than those in summer conditions, but relative humidity becomes higher during winter time. These changes lead to the negative values of calculated latent heat within diurnal cycles in the wintertimes. The model initial values for winter simulations are also listed in Table 1. The initial value of snow isotopic composition ($\delta^{18}O_{s0}$) is the average of precipitation isotopic composition at the starting month for winter season. Due to the lack of observations, $\delta^{18}O_{s0}$ was estimated from the monthly mean temperature and the δ-T slopes in non-summer seasons (0.64±0.02) according to the compiled data in Pang et al. (2019). We also further evaluated these estimations of $\delta^{18}O_{s0}$ by comparison with snowfall $\delta^{18}O$ modelled using the ECWMF5-wiso model (Werner et al., 2011). The initial value for water vapor isotopic composition ($\delta^{18}O_{v0}$) was also estimated assuming isotope equilibrium with $\delta^{18}O_{s0}$. The δf_0 was set to be the calculated $\delta^{18}O_{v0}$ using $\delta^{18}O_{s0}$ and the highest temperature observed in winter during the studied period. The h_0 is kept the same as in summer to simplify the calculations. The median of H_0 at Dome A varies little in most of the year according to Bonner et al. (2009) and Ma B. et al. (2020), so in the model we used the same H_0 in winter as that in summer. The ρ_s is the annual mean snow density based on measurements (Ma T. et al., 2020) and we didn't consider the seasonal variations to simplify the calculations.

带格式的: 字体: 倾斜
带格式的: 字体: Times New Roman
带格式的: 字体: 倾斜
带格式的: 字体: 倾斜
带格式的: 字体: 倾斜, 下标
带格式的: 非上标/ 下标
带格式的: 非突出显示
带格式的: 非突出显示
带格式的: 非突出显示
带格式的: 字体: 倾斜, 非突出显示
带格式的: 字体: 倾斜, 下标, 非突出显示
带格式的: 非突出显示
带格式的: 字体: 倾斜, 非突出显示
带格式的: 非突出显示
带格式的: 字体: 倾斜
带格式的: 字体: 倾斜
带格式的: 字体: 倾斜
带格式的: 字体: 倾斜
带格式的: 字体: 倾斜
带格式的: 字体: 倾斜
带格式的: 字体: 倾斜
带格式的: 字体: 倾斜
带格式的: 字体: 倾斜
带格式的: 字体: 倾斜
带格式的: 字体: 倾斜
带格式的: 字体: 倾斜
带格式的: 字体: 倾斜
带格式的: 字体: 倾斜
带格式的: 非突出显示
带格式的: 非突出显示
带格式的: 字体: 倾斜
带格式的: 非突出显示
带格式的: 非突出显示
带格式的: 字体: 倾斜
带格式的: 字体: 倾斜
带格式的: 非突出显示
带格式的: 非突出显示
带格式的: 字体: 倾斜
带格式的: 字体: 倾斜
带格式的: 字体: 倾斜
带格式的: 字体: 倾斜
带格式的: 字体: 倾斜
带格式的: 非突出显示

2.2.~~3~~4 Sensitivity simulations

Changes in initial parameters could influence the isotopic effects of atmosphere-snow water vapor exchange. For example, previous field experiments indicate that isotopic enrichment caused by atmosphere-snow water vapor exchange tends to decrease with the increase of snow thickness (Hughes et al., 2021). Ritter et al. (2016) pointed out that diurnal variations in water vapor isotopic composition decrease with the increase in mixing layer height (i.e., H_0). These previous findings motivate us to investigate the sensitivity of the modelled results to these boundary conditions and/or initial values.

The sensitivity tests include three~~wo~~ groups of comparative experiments for the Dome A site and run for a 24-h period under summer clear-sky conditions. The first group was focused on the sensitivity of surface and water vapor $\delta^{18}O$ to varying h_0 and H_0. In the experiment, we vary h_0 between 0.1 and 3.0 cm (Ritter et al., 2016; Hughes et al., 2021) and H_0 from 1 to 100 m (Bonner et al., 2009; Fu et al., 2015). The second group was~~is~~ designed for investigating how the uncertainties of $\delta^{18}O_{s0}$ and ~~and~~ $\delta^{18}O_{v0}$, influence the isotopic effects of atmosphere-snow water~~-air~~ vapor exchange, especially when $\delta^{18}O_{s0}$ and $\delta^{18}O_{v0}$ are not equilibrium. We varied the $\delta^{18}O_{s0}$ and ~~and~~ $\delta^{18}O_{v0}$ from -53~~-~~43 ‰ (the range of summer precipitation $\delta^{18}O$ at Dome A, Pang et al. (2019)) and ~~and~~ -855~~-60~~ 55 ‰~~,~~, respectively. The range of $\delta^{18}O_{v0}$ was estimated from $\delta^{18}O_{s0}$ and the equilibrium fractionation coefficient under summer conditions, and $\delta^{18}O_{s0}$ and $\delta^{18}O_{v0}$ in thermodynamic imbalance was included ~~disequilibrium was included~~. The third group respectively varied the $\delta^{18}O_{f0}$ and snow density to test their influence on the diurnal changes in surface snow and water vapor $\delta^{18}O$. The selection~~-~~ of -68~~-~~58 ‰ for the $\delta^{18}O_{f0}$ range is referred to the summer observations of water vapor isotopic composition at Dome C (Casado et al., 2016). According to the field observations at Dome A and other interior domes (Laepple et al., 2018), the range of snow density was set to 300-400 kg/m^3 for sensitivity simulations. Note, the isotope effects are larger in summer than in winter so we only used summer conditions and values to illustrate the sensitivity of the modelled results to theses parameters.

3 Results

3.1 The modelled diurnal cycles at Dome C

The ~~simulated water vapor $\delta^{18}O$ at~~results for Dome C simulations ~~displays an apparent diurnal cycle as~~are shown in Fig. 3, where the mean modelled and observed diurnal patterns of the isotopes are plotted~~a~~. As shown in the figure, water vapor $\delta^{18}O$~~Its value~~ increases from -68 ‰ at 00:00 UTC to -664 ‰ at 093:00 UTC and then decreases to -753 ‰ at 1623:00 UTC. The diurnal ~~variation~~ range of δD is similar to that in $\delta^{18}O$, with a larger peak-valley gap of ~~-30~~ 54 ‰ (Fig. 3b). The water vapor d-excess, defined by d-excess (‰) ≡ δD-8*$\delta^{18}O$ (Dansgaard, 1964), varies between 5234 ‰ and 7265 ‰ during the 24-h period (Fig. 3c). Its diurnal trend is opposite to that of $\delta^{18}O$ and δD. Overall, the modelled diurnal variations of vapor $\delta^{18}O$ and δD capture the observations well, while their magnitudes are slightly larger than those of observations. The modelled snow $\delta^{18}O$ and δD follow a diurnal pattern where higher values occur during the warming phase and lower values during the cooling phase (Fig. 3d). The diurnal range of simulated snow $\delta^{18}O$ are ~2‰ on average. This value is close to the observations in the

带格式的: 字体: 倾斜
带格式的: 字体: 倾斜
带格式的: 字体: 倾斜
带格式的: 字体: 倾斜
带格式的: 字体: 倾斜
带格式的: 字体: 倾斜
带格式的: 字体: 倾斜
带格式的: 字体: 倾斜
带格式的: 字体: 倾斜
带格式的: 字体: 倾斜
带格式的: 字体: 倾斜
带格式的: 字体: 倾斜
带格式的: 字体: 倾斜
带格式的: 非上标/ 下标
带格式的: 字体: 倾斜
带格式的: 字体: 倾斜
带格式的: 上标
带格式的: 上标
带格式的: 字体: (默认) Times New Roman, (中文) Times New Roman

order of magnitude during a typical frost event, but smaller than that of the simulated water vapor $\delta^{18}O$. In addition, ~~The modelled snow $\delta^{18}O$, δD and d-excess also show a diurnal cycle, but their magnitudes in diurnal variations are much smaller than those in water vapor isotopic compositions (Figs. 3a-3e).~~ the diurnal variations in snow d-excess are opposite to that of snow $\delta^{18}O$ and δD (Fig. 3d), like the relationship between vapor $\delta^{18}O$ and d-excess. The model-observation comparisons for the cases at Dome C indicate the model framework can reproduce the observed diurnal variations ~~variations~~ of water vapor isotopes constrained by appropriate meteorological parameters.

3.2 The modelled diurnal cycles at Dome A

3.2.1 Clear-sky conditions

At Dome A, the Richardson number (R_i) varies between -0.01 and 0.02 during the 24-h period (Fig. 4a). The friction velocity of water molecule (u*) ranges from 0.11 to 0.19 m/s, with a mean value of 0.14 m/s (Fig. 4b). The atmosphere~~ir~~-snow water vapor exchange flux (E_x) calculated from R_i and u^* varies in parallel with temperature ~~but lags by ~ 2 h~~ (Fig. 4c). In general, negative R_i values represent relatively unstable atmospheric conditions, and this corresponds to the phase of sublimation (i.e., net vapor flux from snow to the atmosphere~~ir~~, Fig. 4c). In contrast, R_i appears to be positive in most time of the cooling phase (i.e., net vapor flux from atmosphere ~~air~~ to snow, Fig. 4c), suggesting stable atmospheric conditions.

Figs. 4d-4f display the modelled surface snow and water vapor isotopic compositions and the uncertainties. All the isotopes display apparent diurnal cycles. In particular, water vapor $\delta^{18}O$ and δD indicate enrichments in the sublimation period, followed by depletions during the rest of the day when condensation (vapor deposition) dominates (Figs. 4d and 4e). The snow $\delta^{18}O$ and δD exhibit a similar but somewhat opposite pattern within the 24 hours (Figs. 4d and 4e). The diurnal pattern of d-excess is opposite to that of $\delta^{18}O$ and δD in snow and vapor~~air~~ (Fig. 4f). In all, the diurnal patterns of snow and water vapor isotopes at Dome A are similar to those at Dome C during summer cloudless conditions.

The magnitudes of the diurnal ~~variations~~ range in water vapor isotopic composition are ~~8.15~~4.75 ‰ for $\delta^{18}O$, 28.78~~54.44~~ ‰ for δD and ~~14.82~~9.25 ‰ for d-excess. In comparison, the modelled diurnal isotope variations in surface snow are much smaller with magnitudes of ~~0.11~~0.80 ‰ for $\delta^{18}O$, ~~0.62~~1.64 ‰ for δD and ~~0.29~~4.85 ‰ for d-excess. In addition, after 24-hour model running, the water vapor $\delta^{18}O$ ~~and~~, δD, and d-excess ~~decrease~~increase by ~~7.62~~2.35 ‰~~ and~~, ~~50.04~~15.67 ‰, and 3.13 ‰, respectively~~, whereas its d-excess increases by 10.95 ‰ compared to the initial value~~ (Figs. 4d-4f). Meanwhile, after 24 hours, the snow isotopic compositions display enrichments of 0.~~09~~29 ‰ for $\delta^{18}O$ and 1.09~~0.52~~ ‰ for δD, and a depletion of 1.26~~0.19~~ ‰ for d-excess.

3.2.2 Highly cloudy conditions

During highly cloudy conditions, the Richardson number (R_i) is almost neutral or unstable at the diurnal scale (Fig. 5a). While the friction velocity (u*) exhibits a diurnal cycle varying between 0.11 m/s and 0.13 m/s (Fig. 5b), which is much smaller than

带格式的: 英语(英国)

带格式的: 字体: 倾斜

带格式的: 字体: 倾斜

带格式的: 字体: 倾斜

带格式的: 字体: 倾斜

带格式的: 字体: (默认) Times New Roman, (中文) Times New Roman

带格式的: 字体: (默认) Times New Roman, (中文) Times New Roman

that under clear-sky conditions. We also find the diurnal cycle in atmosphere-snow water vapor exchange flux (E_x), as shown in Fig. 5c. Overall, the diurnal changes in u^*, R_i and E_x are less pronounced compared with those under clear-sky conditions. The diurnal cycle pattern in water and surface snow isotopic composition is also apparent under cloudy conditions (Figs. 5d-5f), but the magnitudes are smaller than those under clear-sky conditions. In particular, the diurnal peak-to-valley difference of water vapor isotopic composition is ~~5.43~~3.00 ‰ for $\delta^{18}O$, ~~35.72~~21.15 ‰ for δD and ~~7.95~~4.02 ‰ for d-excess. The diurnal variations in surface snow isotopic composition have a magnitude of 0.~~04~~ 28 ‰ for $\delta^{18}O$, 0.~~25~~ 87 ‰ for δD, ~~0.10~~2.21 ‰ for d-excess. In addition, the same as in clear-sky conditions, after 24-hours, snow water isotopes were enriched in the model.

3.3 The modelled diurnal cycles under Dome A winter conditions

The winter simulation results are plotted in Fig. 6. Under winter conditions, the Richardson number (Ri) and the friction velocity (u*) keep stable in a full 24-hour period (Figs. 6a and 6b). The atmosphere-snow water vapor exchange flux (E_x) show negative values throughout the 24 hours (Fig. 6c), suggesting that sublimation does not occur under Dome A winter conditions. As a result, in comparison with the simulated results in summer, there is no significant diurnal variations in snow isotopes in winter, but the changes in water vapor isotopic composition in winter are comparable to the ones in summer. ~~As a result, compared to the simulated results in summer, there is no diurnal cycles in water vapor and snow isotopes in winter.~~ This can be associated with the almost unchanged meteorological conditions and the relatively weak exchange between snow and atmospheric water vapor during a diurnal period, as displayed Fig. 2c. In addition, because the isotopic composition in deposited vapor are much lower than that in surface snow, the winter snow layer experiences small but steady depletions in $\delta^{18}O$ and δD (Figs. 6d and 6e). In contrast, snow d-excess becomes more enriched under the effects of atmosphere-snow water vapor exchange flux (Fig. 6f). The water vapor isotopic composition also display a depletion because heavier isotopes tend to deposit faster.

3.4 Sensitivity to model parameters

The results of sensitivity tests are shown in Fig. 7. As shown in the figure, the magnitude of the diurnal variations in water vapor $\delta^{18}O$ ($\delta^{18}O_v$) is very sensitive to H_0 but not to h_0 (Fig. 7a) given that H_0 determines the atmospheric water reservoir. This is consistent with Ritter et al. (2016) who pointed out that diurnal variations in water vapor isotopic composition decrease with the increase of mixing layer height. In contrast, the magnitude of diurnal variations in snow $\delta^{18}O$ ($\delta^{18}O_s$) is more sensitive to h_0 (Fig. 7b). This is also consistent with field experiments that indicate that isotopic enrichment caused by atmosphere-snow water vapor exchange tends to decrease with the increase of snow thickness (Hughes et al., 2021).

In Figure 7, we also plotted the modelled magnitude of diurnal cycles (Figs. 7d~~e~~ and 7e~~d~~) and the changes in $\delta^{18}O_s$ ~~and $\delta^{18}O_v$~~ after a diurnal cycle (Figs. ~~7e and~~ 7f). As shown in the figures, within the realistic $\delta^{18}O_{s0}$ and $\delta^{18}O_{v0}$ ranges, the magnitude of $\delta^{18}O_v$ diurnal cycle ~~and its value after a diurnal cycle~~ is more sensitive to $\delta^{18}O_{v0}$ than $\delta^{18}O_{s0}$. The magnitude of $\delta^{18}O_s$ becomes smaller with the decrease ~~of $\delta^{18}O_{v0}$ and~~ of $\delta^{18}O_{s0}$ (< 0.~~00~~305‰)~~, but such a change is negligible (< 0.001‰)~~. The value of

带格式的: 字体: 倾斜
带格式的: 字体: 倾斜
带格式的: 字体: 倾斜
带格式的: 字体: 倾斜
带格式的: 字体: 倾斜
带格式的: 字体: 倾斜
带格式的: 字体: 倾斜
带格式的: 字体: 倾斜
带格式的: 字体: 倾斜
带格式的: 字体: 倾斜
带格式的: 非突出显示
带格式的: 字体: 倾斜
带格式的: 非突出显示

$\delta^{18}O_s$ after a diurnal simulation ~~cycle~~ is also more ~~neither~~ sensitive to $\delta^{18}O_{w0}$ ~~nor $\delta^{18}O_{s0}$~~, but such a change is very small (<0.01‰)~~even when disequilibrium between snow and vapor water isotopes occurs (the equilibrium line in Fig. 7f)~~.
The changes in $\delta^{18}O_{f0}$ can significantly affect the magnitude of the diurnal variations in $\delta^{18}O_v$, as shown in Fig. 7g. However, there is a lesser impact on the magnitude of diurnal $\delta^{18}O_s$ variations and $\Delta_{s}\delta^{18}O_{ds}$ changes after a diurnal cycle (Fig. 7h and 7i). The snow density has a considerable effect on $\Delta_{s}\delta^{18}O_{ds}$, but it causes only a limited change in the magnitude of diurnal $\Delta_{s}\delta^{18}O_{ds}$ variations.

4 Discussion

Although with differences on the magnitudes, under summer clear-sky and highly cloudy conditions the modelled isotopes in surface snow and water vapor display clear diurnal ~~cycles~~patterns at Dome A. At all these two cases ~~exhibiting a diurnal cycle~~, the water vapor isotopes show a smaller magnitudes of diurnal variations with respect to those in snow isotopes. In general, in the period of mass exchange dominated by sublimation, snow $\delta^{18}O$ and δD are enriched as lighter isotopes are preferentially sublimated to the atmosphere. Meanwhile, sublimates mixing with vapor water lead to increases in vapor $\delta^{18}O$ and δD because ~~the factor~~ the sublimates are of higher $\delta^{18}O$ and δD than atmospheric vapor ~~given the starting materials (i.e., surface snow) are of high $\delta^{18}O$ and δD~~. In the period of mass exchange dominated by deposition, vapor water $\delta^{18}O$ and δD are depleted significantly. Note that~~but~~ the effects on snow $\delta^{18}O$ and δD are ~~very~~ smaller than those on vapor $\delta^{18}O$ and δD. This~~e latter~~ is due to the fact that surface snow mass reservoir is much larger than to the mass of deposition, so that the associated isotope effects on surface snow are ~~negligible~~very small.

Based on Fig. 2, 4c, and 5c, it is clear that the diurnal isotope cycles in surface snow and vapor water have a strong correlation with surface temperature and humidity. ~~It is evident from Fig. 2, 4c and 5c that the diurnal isotope cycles in surface snow and vapor water are probably controlled by temperature and humidity.~~ As described in Section 2.1, surface temperature can modify local atmospheric dynamical conditions and specific humidity, leading to synchronous responses in atmosphere-snow water vapor exchange flux. Temperature can also affect isotope fractionation during phase exchange. Atmosphere-snow water vapor exchange is associated with equilibrium and kinetic isotope fractionations between snow and water vapor (Ritter et al., 2016; Hughes et al., 2021; Wahl et al., 2021). The degree of isotopic equilibrium fractionation is directly dependent on local surface temperature (Ellehoj et al., 2013), while kinetic isotope fractionation is mainly driven by the vapor pressure gradient between snow surface and atmosphere (Jouzel & Merlivat, 1984; Surma et al., 2021; Passey & Levin, 2021). Specific humidity is also important as it represents the size of the water vapor reservoir which snow can exchange with (Casado et al., 2018). But it is only important for atmospheric vapor $\delta^{18}O$ and δD as surface snow is a much larger mass reservoir which buffers the effects of atmospheric vapor change. Wind speed also ~~may~~ play a key role in driving isotopic ~~cycles~~ variations ~~in the coastal sites where strong katabatic winds are visible (Bréant et al., 2019), but~~ at Dome A, because it can enlarge the variations in latent

带格式的: 非突出显示
带格式的: 非突出显示
带格式的: 字体: 倾斜
带格式的: 字体: 倾斜, 非突出显示
带格式的: 字体: 倾斜
带格式的: 非突出显示
带格式的: 字体: 倾斜
带格式的: 字体: 倾斜
带格式的: 字体: 倾斜
带格式的: 字体: 倾斜
带格式的: 字体: 倾斜, 上标
带格式的: 字体: 倾斜
带格式的: 字体: 倾斜, 下标
带格式的: 字体: 倾斜
带格式的: 字体: 倾斜
带格式的: 字体: 倾斜, 上标
带格式的: 字体: 倾斜
带格式的: 字体: 倾斜, 下标
带格式的: 字体: 倾斜
带格式的: 字体: 倾斜, 上标
带格式的: 字体: 倾斜
带格式的: 字体: 倾斜, 下标
带格式的: 下标
带格式的: 字体: (默认) Times New Roman, (中文) Times New Roman
带格式的: 非突出显示
带格式的: 非突出显示
带格式的: 非突出显示
带格式的: 段落间距段前: 0 磅
带格式的: 非突出显示
带格式的: 非突出显示
带格式的: 非突出显示

heat, leading to a more significant diurnal change in water vapor isotopes and snow isotopes.~~appears the diurnal cycle of the wind speed is too little to significantly affect diurnal isotopic cycles of water vapor and snow.~~

We also compared our modelled water vapor $\delta^{18}O$, δD, and d-excess data at Dome A simulations with those water vapor $\delta^{18}O$, δD, and d-excess data from other East Antarctic interior sites from observations, such as Kohnen station, Dome C, and a location about 100 km away from Dome A (Ritter et al., 2016; Casado et al., 2016; Liu et al., 2022). In general, both our simulations and observations show diurnal patterns, with high values during the daytime warming phase and low values during the night-time cooling phase. However, we noticed that the observed diurnal changes in water vapor $\delta^{18}O$ and d-excess at sites near Dome A are very large, over 40‰ and 200‰, respectively. This is probably could be due to calibration drifts caused by the extremely cold and dry conditions during the measurements at the nearest Dome A site which influence the measurements (Liu et al., 2022). The averaged δD observations of 36±6‰ at Kohnen station and the in-situ measurements of 38±2‰ at Dome C are higher than our modelled δD value of 28.78±19.06‰ at Dome A. This difference can be attributed to atmospheric dynamical conditions linked with wind speed in addition to other meteorological conditions. At Dome A, the daily mean wind speed of 2.8 m/s is lower than 3.3 m/s in Dome C and 4.5 m/s in Kohnen station during summer. A lower wind speed corresponds to relatively weak air convection in the horizontal orientation. Due to the coupling between upper and lower atmospheric layers, vertical turbulent mixing may decrease with the weakened air convection in the atmospheric near-surface layer (Casado et al., 2018). This change can attenuate molecular exchange between surface snow and water vapor. In parallel, the decrease of vertical turbulence may result in a less efficient turbulent diffusion of water molecules and an elevated contribution of molecular diffusion during atmosphere-snow water vapor exchange. Changes in water vapor diffusion pathways increase kinetic fractionation and reduce effective isotopic fractionation of water isotopes, leading to a muted fluctuation of modelled water vapor δD in combination with less mass exchange.

~~As described in Section 2.1, temperature can modify local atmospheric dynamical conditions and specific humidity, leading to synchronous responses in atmosphere-snow water vapor exchange flux.~~

~~Temperature also affects isotope fractionation during phase exchange. Atmosphere-snow water vapor exchange is associated with equilibrium and kinetic isotope fractionations between snow and water vapor (Ritter et al., 2016; Hughes et al., 2021; Wahl et al., 2021). The degree of isotopic equilibrium fractionation is directly dependent on local temperature (Ellehoj et al., 2013), while kinetic isotope fractionation is mainly driven by the vapor pressure gradient between snow surface and air (Jouzel & Merlivat, 1984; Surma et al., 2021; Passey & Levin, 2021). Specific humidity is also important as it represents the size of the water vapor reservoir which snow can exchange with (Casado et al., 2018). But it is only important for atmospheric vapor $\delta^{18}O$ and δD as surface snow is a much larger mass reservoir which buffers the effects of atmospheric vapor change.~~

The magnitudes of modelled diurnal changes in snow $\delta^{18}O$ and δD are different between the highly cloudy and clear-sky conditions, with apparently small magnitudes under cloudy conditions. It seems when cloud is present, surface snow will receive longwave radiation from the cloud and be less influenced by solar radiation. As a result, the diurnal radiation budget cycle is less variable compared to days without cloud as otherwise solar radiation with strong diurnal cycle become the only

带格式的：上标
带格式的：上标
带格式的：上标
带格式的：段落间距段前: 6 磅

players. In days with cloud, diurnal variations of air temperature and surface temperature are also smaller (Fig. 2). With the presence of cloud, the differences between the air temperature and surface temperature during the day and night become less pronounced (as shown in Fig. 2). This could have a negative impact on the changes in atmospheric dynamics between day and night, as evidenced by the relatively small magnitude of diurnal variations in Richardson number (as shown in Figs. 4a and 5a).~~This could adversely affect changes in atmospheric dynamical conditions between day and night, as evidenced by a relatively small magnitude of diurnal variations in Richardson number (Figs. 4a and 5a).~~ Diurnal variations in wind speed and friction velocity are thus not significant (Figs. 2, 4b, and 5b). As a result, vertical turbulent mixing between surface snow and water vapor in a diurnal cycle is relative stable, leading to less mass exchange as well as isotope effects between the two reservoirs.

The model results for summer clear-sky and highly cloudy conditions also indicate that after a 24-hour simulation~~full diurnal cycle~~, $\delta^{18}O$ and δD in surface snow are enriched mainly due to isotope fractionations during sublimation, while that in atmospheric vapor are depleted mainly due to isotope fractionations during deposition. Note, although in the period dominated by deposition, vapor water with much lighter $\delta^{18}O$ and δD than snow are deposited, the mass are negligible compared to the snow mass reservoir so that the effects on snow isotopes in the 24-hour simulation period are dominated by the effects of sublimation. The enrichments in snow isotopes caused by sublimation are consistent with previous studies (e.g., Ritter et al., 2016; Casado et al., 2018; Hughes et al., 2021). In addition, sublimation is associated with snow mass loss. Many studies also indicate significant surface snow mass loss during summer due to sublimation at inland Antarctic sites including Dome A (e.g., Frezzotti et al., 2004; Ding et al., 2016). As such, at Dome A, surface snow isotopes would be presumably enriched during summer. Using a simple Rayleigh distillation model, Pang et al. (2019) predicted that over summer ~2 ‰ enrichments in surface snow $\delta^{18}O$ can be caused under mean Dome A summer conditions.

In comparison, under Dome A typical winter conditions, temperature and humidity are relatively constant during a day (i.e., 24-hour simulation period), and the R_i is positive throughout a day, indicating stable atmospheric conditions. Consequently, less clear~~no~~ diurnal variations ~~cycles~~ in atmosphere~~ir~~-snow water vapor exchange can be caused, so as the isotopes. In particular, the model indicates in winter only deposition can occur and which leads to more or less snow isotope depletion ($\delta^{18}O$ and δD) after the 24-hour simulation period.

Because the diurnal magnitude in snow isotopic composition induced by atmosphere-snow water vapor exchange~~air-snow exchange~~ in summer and winter are different, the seasonal snow isotope variations can be affected. In particular, according to the modelled results, in summer surface snow $\delta^{18}O$ and δD would become enriched compared to fresh snow, while in winter surface snow isotopes would be depleted compared to fresh snow. As a result, an amplification of the snow isotope seasonality would be caused by the atmospheric vapor-snow exchange. This effect appears to be distinct from what can be expected by other post-depositional processes. For example, Town et al. (2008) have demonstrated that wind-driven ventilation after snowfall can result in isotope enrichment of winter snow layers and depletion of summer snow layers, decreasing the magnitude of seasonal variations. Vapor diffusion in snow pore also contributes to the attenuation of the $\delta^{18}O$ or δD seasonal variations by smoothing (Johnsen et al., 2000; Casado et al., 2020). In terms of evaluating the annual net effect of atmospheric~~- vapor-~~

snow vapour exchange, potential mass loss in summer and gain in winter have to estimated, but from the results of this study it appears the annual net effects would be small due the offsetting effects in summer and winter.

5 Conclusions

Atmosphere-snow water vapor exchange is important for snow isotopes preservations as suggested by previous studies (Ritter et al., 2016; Hughes et al., 2021; Hu et al., 2022). In this study, we constructed a new box model based on the bulk aerodynamic method to predict changes in surface snow and water vapor isotopic compositions in response to diurnal fluctuations in local meteorological conditions. The model was validated by agreements between the modelled and observed diurnal cycles of water vapor $\delta^{18}O$, δD, and d-excess at Dome C and then applied to investigate the degree of atmosphere-snow water vapor exchange and the associated isotope effects at Dome A on the diurnal scales. The model results show that atmosphere-snow water vapor exchange at Dome A can also lead to similar diurnal isotope variations in atmospheric water vapor $\delta^{18}O$ and δD under summer conditions, with corresponding diurnal variations in surface snow $\delta^{18}O$ and δD. For the case with clear-sky conditions, the magnitudes of diurnal cycles in snow and water vapor isotopes are larger than those simulations with highly cloudy conditions. In addition, we performed diurnal simulations under Dome A winter conditions. The results indicate the ~~there is no~~ diurnal isotope variations~~cycles~~ over the 24-hour simulation period is less significant due to the stable atmospheric conditions with low and relative stable air temperature and specific humidity there. However, the model results suggest there is snow isotope depletion can be caused in winter. The modelled opposite isotope effects on snow after 24-hour in winter and summer at Dome A suggest that atmosphere-snow water vapor exchange~~air-snow exchange~~ could enlarge the seasonal snow isotope variations, but may have a mall annual net effect given the offsetting effects in summer and winter. This remains to be further explored with model simulations and validated by observations.

We also wanted to acknowledge the limitations inherent to our simulations with one-dimensional model. The air -mass ~~renewal~~ advection process between free atmospheric layer and boundary layer may play an important role in the atmosphere-snow water vapor exchange as observed during some frost events (Casado et al., 2018). Although the impact of air mass advection process has been incorporated into~~, but it has not been incorporated into~~ our model, it is worth to refine the underlying assumptions for air mass advection process and then improve the accuracy of model simulations. On the other hand, observational validation of the model results for winter season ~~conditions~~ yet unavailable due to~~, because~~ the extreme harsh conditions at Dome A~~, especially for winter season~~. Although it is currently difficult to conduct field work at diurnal scale there, observations on longer timescales (e.g., weekly resolved sampling of surface snow and precipitations over a year along with a snowpack to reconstruct the changes after deposition) could be possible. These are important to validate the model's prediction on the associated isotope effects of atmosphere-snow water vapor exchange~~air-snow vapor exchange~~, especially considering the model implies atmosphere-snow water vapor exchange~~air-snow vapor exchange~~ may have little isotope effects at the annual scale but tend to enlarge snow water isotope seasonality. The latter is opposite to other post-depositional processes such as wind-driven ventilation (Town et al., 2008) and vapor diffusion in snow pore (Johnsen et al., 2000).

带格式的：非突出显示

带格式的：非突出显示

带格式的：非突出显示

Data Availability Statement

The simulated data and model code are available by request to Tianming Ma (Email: mtm@ustc.edu.cn). Other data and software used in this study are also available online. We also acknowledge using Dome C data from the CALVA project and CENECLAM and GLACIOCLIM observatories (http://www-lgge.ujf-grenoble.fr/~christo/calva/). ~~Meteorological observations at Dome C are provided in CALVA program (https://web.lmd.jussieu.fr/~egenthon/SiteCALVA/CalvaData).~~ Meteorological observations at Dome A can be downloaded at Australian Antarctic Data Centre (https://data.aad.gov.au/metadata/records/DomeA_AWS). The hourly averages of total cloud cover and longwave radiative fluxes are sourced from ERA5 reanalysis dataset (https://cds.climate.copernicus.eu/cdsapp#!/dataset/reanalysis-era5-single-levels). ~~The Matlab code for uncertainty analysis are obtained from https://www.mathworks.com/matlabcentral/fileexchange/89812-uncertainty-propagation-functions (Klebba, 2022).~~

Author contributions.

LG and TM conceived this study. TM performed the model simulations, analyzed the data and wrote the manuscript with LG. LG and JZ provided helping with the model construction. MD, WZ and YL provided available data for the model driven. All authors contributed to data interpretation and writing

Competing interests.

The authors declare that there is no conflict of interest.

Acknowledgments.

The research leading to these results has received the financial support from National Natural Science Foundation of China (No. 42206242 to T. M.), the State Key Laboratory of Cryospheric Science for the Open fund (SKLCS-OP-2020-06 to T. M.), the Nature Science Research Project of Anhui province (2108085QD158 to T. M.), and the Fundamental Research Funds for the Central Universities. L.G. acknowledges financial support from the National Natural Science Foundation of China (Awards: 41822605, 41871051 and 41727901), the Fundamental Research Funds for Central Universities, the Strategic Priority Research Program of Chinese Academy of Sciences (XDB 41000000), and the National Key R&D Program of China (2019YFC1509100). This research was also supported in part by National Natural Science Foundation of China (49973006, 40773074 and 40703019 to Y. ~~S.~~ L.) and Ministry of Science and Technology of China (2006BAB18B01 to Y. ~~S.~~ L.). The authors are grateful for data collection by Chinese National Antarctic Research Expedition during the summer of 2005-2011.

带格式的：默认段落字体

带格式的：突出显示

References

An, C., Hou, S., Jiang, S., Li, Y., Ma, T., Curran, M. A. J., et al.: The long-term cooling trend in East Antarctic Plateau over the past 2000 years is only robust between 550 and 1550 CE, Geophysical Research Letters, 48, e2021GL092923, doi: 10.1029/2021GL092923, 2021.

Anderson, P. S.: A Method for Rescaling Humidity Sensors at Temperatures Well below Freezing, Journal of Atmospheric and Oceanic Technology, 11(5), 1388-1391, doi: 10.1175/1520-0426(1994)011<1388:AMFRHS>2.0.CO;2, 1994.

Berkowicz, R., & Prahm, L. P.: Evaluation of the profile method for estimation of surface fluxes of momentum and heat, Atmosphere Environment, 16(12), 2809-2819, doi: 10.1016/0004-6981(82)90032-4, 1982.

Bonner, C. S., Ashley, M. C. B., Cui, X., Feng, L., Gong, X., Lawrence, J. S., et al.: Thickness of the atmospheric boundary layer above Dome A, Antarctica, during 2009, Publications of the Astronomical Society of the Pacific, 122, 1122-1131, doi: 10.1086/656250, 2010.

Bo, S., Siegert, M., Mudd, S., Sugden, D., Fujita, S., & Xiangbing, C. The Gamburtsev mountains and the origin and early evolution of the Antarctic Ice Sheet, Nature, 459, 690-693, doi: 10.1038/nature08024, 2009.

Bréant, C., Leroy Dos Santos, C., Agosta, C., Casado, M., Fourré, E., Goursaud, S., et al.: Coastal water vapor isotopic composition driven by katabatic wind variability in summer at Dumont d'Urville, coastal East Antarctica, Earth and Planetary Science Letters, 514, 37-47. doi: 10.1016/j.epsl.2019.03.004, 2019.

Brun, E., Six, D., Picard, G., Vionnet, V., Arnaud, L., Bazile, E., et al: Snow/atmosphere coupled simulation at Dome C, Antarctica, Journal of Glaciology, 57(204), 721-736, doi: 10.3189/002214311797409794, 2011.

Casado, M., Landais, A., Masson-Delmotte, V., Genthon, C., Kerstel, E., Kassi, S., et al: Continuous measurements of isotopic composition of water vapour on the East Antarctic Plateau, Atmospheric Chemistry and Physics, 16(13), 8521-8538, doi: 10.5194/acp-16-8521-2016, 2016.

Casado, M., Landais, A., Picard, G., Münch, T., Laepple, T., Stenni, B., et al.: Archival processes of the water stable isotope signal in East Antarctic ice cores, The Cryosphere, 12(5), 1745-1766, doi: 10.5194/tc-12-1745-2018, 2018.

Casado, M., Münch, T., & Laepple, T. Climatic information archived in ice cores: impact of intermittency and diffusion on the recorded isotopic signal in Antarctica, Climate of the Past, 16, 1581-1598, doi: 10.5194/cp-16-1581-2020, 2020.

Craig, H.: Isotope Variations in Meteoric Waters, Science, 133(3465), 1702-1703, doi: 10.1126/science.133.3465.1702, 1961.

Champollion, N., Picard, G., Arnaud, L., Lefebvre, É., Macelloni, G., Rémy, F., and Fily, M.: Marked decrease in the near-surface snow density retrieved by AMSR-E satellite at Dome C, Antarctica, between 2002 and 2011, The Cryosphere, 13, 1215–1232, https://doi.org/10.5194/tc-13-1215-2019, 2019.

Dansgaard, W.: Stable isotopes in precipitation, Tellus, 16(4), 436-468, doi: 10.1111/j.2153-3490.1964.tb00181.x, 1964.

Dansgaard, W., Johnsen, S., Clausen, H., & Gundestrup, N.: Stable isotope glaciology, Meddelelser om Gronland, 197, 1-53.

Ding, M., Xiao, C., Yang, Y., Wang, Y., Li, C., Yuan, N., et al.: Re-assessment of recent (2008-2013) surface mass balance over Dome Argus, Antarctica, Polar Research, 35(1), 26133, doi: 10.3402/polar.v35.26133, 2016.

带格式的：字体: Times New Roman, 10 磅, 字体颜色: 自动设置, 图案: 清除

Ebner, P. P., Steen-Larsen, H. C., Stenni, B., Schneebeli, M., & Steinfeld, A.: Experimental observation of transient δ18O interaction between snow and advective airflow under various temperature gradient conditions, The Cryosphere, 11(4), 1733-1743, doi: 10.5194/tc-11-1733-2017, 2017.

Ekaykin, A. A., Vladimirova, D. O., Lipenkov, V. Y., & Masson-Delmotte, V.: Climatic variability in Princess Elizabeth Land (East Antarctica) over the last 350 years, Climate of the Past, 13, 61-71, doi: 10.5194/cp-13-61-2017, 2017.

Ellehoj, M. D., Steen-Larsen, H. C., Johnsen, S. J., & Madsen, M. B.: Ice-vapor equilibrium fractionation factor of hydrogen and oxygen isotopes: experimental investigations and implications for stable water isotope studies, Rapid Communications in Mass Spectrometry, 27(19), 2149-2158, doi: 10.1002/rcm.6668, 2013.

EPICA community members: Eight glacial cycles from an Antarctic ice core, Nature, 429(6992), 623-628, doi: 10.1038/nature02599, 2004.

Fujita, K., & Abe, O.: Stable isotopes in daily precipitation at Dome Fuji, East Antarctica, Geophysical Research Letters, 33(18), L18503, doi:10.1029/2006gl026936, 2006.

Genthon, C., Town, M. S., Six, D., Favier, V., Argentini, S., & Pellegrini, A.: Meteorological atmospheric boundary layer measurements and ECMWF analyses during summer at Dome C, Antarctica, Journal of Geophysical Research: Atmospheres, 115, D05104, doi: 10.1029/2009JD012741, 2010.

Genthon, C., Piard, L., Vignon, E., Madeleine, J.-B., Casado, M., & Gallée, H.: Atmospheric moisture supersaturation in the near-surface atmosphere at Dome C, Antarctic Plateau, Atmospheric Chemistry and Physics, 17(1), 691-704, doi: 10.5194/acp-17-691-2017, 2017.

Haynes, J. M., Vonder Haar, T. H., L'Ecuyer, T., & Henderson, D. Radiative heating characteristics of earth's cloudy atmosphere from vertically resolved active sensors, Geophysical Research Letters, 40, 624-630, doi: 10.1002/grl.50145, 2013.

Holtslag, A. A. M. & De Bruin, H. A. R.: Applied modeling of the nighttime surface energy balance over land, Journal of Applied Meteorology and Climatology, 27(6), 689-704, doi: 10.1175/1520-0450(1988)027<0689:AMOTNS>2.0.CO;2, 1988.

Hoshina, Y., Fujita, K., Nakazawa, F., Iizuka, Y., Miyake, T., Hirabayashi, M., et al.: Effect of accumulation rate on water stable isotopes of near-surface snow in inland Antarctica, Journal of Geophysical Research: Atmospheres, 119(1), 274-283, doi: 10.1002/2013jd020771, 2014.

Hou, S., Wang, Y., & Pang, H.: Climatology of stable isotopes in Antarctic snow and ice: Current status and prospects, Chinese Science Bulletin, 58(10), 1095-1106, doi: 10.1007/s11434-012-5543-y, 2012.

Hu, J., Yan, Y., Yeung, Y., & Dee, S: Sublimation Origin of Negative Deuterium Excess Observed in Snow and Ice Samples from McMurdo Dry Valleys and Allan Hills Blue Ice Areas, East Antarctica, Journal of Geophysical Research: Atmosphere, 127, e2021JD035950, doi: 10.1029/2021JD035950, 2022.

Hu, Z., Shi, G., Talalay, P., Li, Y., Fan, X., An, C. et al.: Deep ice-core drilling to 800 m at Dome A in East Antarctica, Annals of Glaciology, 62(85-86), 293-304, doi: 10.1017/aog.2021.2, 2021.

Hughes, A. G., Wahl, S., Jones, T. R., Zuhr, A., Hörhold, M., White, J. W. C., et al.: The role of sublimation as a driver of climate signals in the water isotope content of surface snow Laboratory and field experimental results, The Cryosphere, 15(10), 4949-4974, doi:10.5194/tc-15-4949-2021, 2021.

Jiang, S., Cole-Dai, J., Li, Y., Ferris, D. G., Ma, H., An, C., et al.: A detailed 2840 year record of explosive volcanism in a shallow ice core from Dome A, East Antarctica, Journal of Glaciology, 58(207), 65-75, doi: 10.3189/2012JoG11J138, 2012.

Johnsen, S., Clausen, H. B., Cuffey, K. M., Hoffmann, G., Schwander, J., & Creyts, T.: Diffusion of stable isotopes in polar firn and ice: the isotope effect in firn diffusion, Physics of ice core records, pp. 121-140, 2000.

Jouzel, J., & Merlivat, L.: Deuterium and oxygen 18 in precipitation: Modeling of the isotopic effects during snow formation, Journal of Geophysical Research: Atmospheres, 89(D7), 11749-11757, doi: 10.1029/JD089iD07p11749, 1984.

Klebba, J.: Uncertainty Propagation Functions. MATLAB Central File Exchange [Software], https://www.mathworks.com/matlabcentral/fileexchange/89812-uncertainty-propagation-functions.

Laepple, T., Münch, T., Casado, M., Hoerhold, M., Landais, A., & Kipfstuhl, S.: On the similarity and apparent cycles of isotopic variations in East Antarctic snow pits, The Cryosphere, 12(1), 169-187, doi: 10.5194/tc-12-169-2018, 2018.

Li, C., Ren, J., Shi, G., Pang, H., Wang, Y., Hou, S., et al.: Spatial and temporal variations of fractionation of stable isotopes in East-Antarctic snow, Journal of Glaciology, 67(263), 523-532, doi: 10.1017/jog.2021.5, 2021.

Lorius, C., Merlivat, L. & Hagemann R.: Variation in the mean deuterium content of precipitations in Antarctica, Journal of Geophysical Research, 74, 7027–7031, doi: 10.1029/JC074i028p07027, 1969.

Ma, B., Shang, Z., Hu, Y., Hu, K., Wang, Y., Yang, X., et al.: Night-time measurements of astronomical seeing at Dome A in Antarctica, Nature, 583(7818), 771–774, doi: 10.1038/s41586-020-2489-0, 2020.

Ma, T., Li, L., Li, Y., An, C., Yu, J., Ma, H., et al.: Stable isotopic composition in snowpack along the traverse from a coastal location to Dome A (East Antarctica): Results from observations and numerical modelling, Polar Science, 24, 100510, doi: 10.1016/j.polar.2020.100510, 2020.

Ma, Y., Bian, L., Xiao, C., Allison, I., & Zhou, X., Near surface climate of the traverse route from Zhongshan Station to Dome A, East Antarctica, Antarctic Science, 22(4), 443-459, doi: 10.1017/s0954102010000209, 2010.

Madsen, M. V., Steen-Larsen, H. C., Horhold, M., Box, J., Berben, S. M. P., Capron, E., et al.: Evidence of Isotopic Fractionation During Vapor Exchange Between the Atmosphere and the Snow Surface in Greenland, Journal of Geophysical Research: Atmospheres, 124(6), 2932-2945, doi: 10.1029/2018JD029619, 2019.

Makkonen, L.: Comments on ‘‘A Method for Rescaling Humidity Sensors at Temperatures Well below Freezing, Journal of Atmospheric and Oceanic Technology, 13(4), 911-912, doi: 10.1175/1520-0426(1996)013<0911:COMFRH>2.0.CO;2, 1996.

Makkonen, L., & Laakso, T.: Humidity Measurements in Cold and Humid Environments, Boundary-Layer Meteorology, 116(1), 131-147, doi:10.1007/s10546-004-7955-y, 2005.

Masson-Delmotte, V., Hou, S., Ekaykin, A., Jouzel, J., Aristarain, A., Bernardo, R. T., et al.: A review of Antarctic surface snow isotopic composition: observations, atmospheric circulation, and isotopic modeling, Journal of Climate, 21, 3359-3387. doi: 10.1175/2007jcli2139.1, 2008.

Markle, B. R., & Steig, E. J.: Improving temperature reconstructions from ice-core water-isotope records, Climate of the Past, 18, 1321-1368, doi: 10.5194/cp-18-1321-2022, 2022.

Merlivat, L., & Jouzel, J.: Global climatic interpretation of the deuterium-oxygen 18 relationship for precipitation, Journal of Geophysical Research: Oceans, 84(C8), 5029, doi: 10.1029/JC084iC08p05029, 1979.

Monin, A. S., & Obukhov, A. M.: Basic laws of turbulent mixing in the atmosphere near the ground, Tr. Geophiz. Inst. Akad. Nauk. SSSR, 24(151), 163-187, 1954.

Neumann, T. A., Albert, M. R., Engel, C., Courville, Z., & Perron, F.: Sublimation rate and the mass-transfer coefficient for snow sublimation, International Journal of Heat and Mass Transfer, 52(1-2), 309-315, doi: 10.1016/j.ijheatmasstransfer.2008.06.003, 2009.

Pang, H., Hou, S., Landais, A., Masson-Delmotte, V., Jouzel, J., Steen-Larsen, H. C.: Influence of Summer Sublimation on δD, δ18O, and δ17O in Precipitation, East Antarctica, and Implications for Climate Reconstruction from Ice Cores, Journal of Geophysical Research: Atmospheres, 124(13), 7339-7358, doi: 10.1029/2018JD030218, 2019.

Passey, B. H., & Levin, N. E.: Triple Oxygen Isotopes in Meteoric Waters, Carbonates, and Biological Apatites: Implications for Continental Paleoclimate Reconstruction, Reviews in Mineralogy and Geochemistry, 86(1), 429-462, doi: 10.2138/rmg.2021.86.13, 2021.

Petit, J. R., Jouzel, J., Raynaud, D., Barkov, N. I., Barnola, J. M., Basile, I., et al.: Climate and atmospheric history of the past 420,000 years from the Vostok ice core, Antarctica, Nature, 399(6735), 429-436, doi: 10.1038/20859, 1999.

Qian, Y., Long, C. N., Wang, H., Comstock, J. M., Mcfarlane, S. A., & Xie, S.: Evaluation of cloud fraction and its radiative effect simulated by IPCC AR4 global models against ARM surface observations, Atmospheric Chemistry and Physics, 12(4), 1785-1810, doi: 10.5194/acp-12-1785-2012, 2012.

Radić, V., Menounos, B., Shea, J., Fitzpatrick, N., Tessema, M. A., & Déry, S. J.: Evaluation of different methods to model near-surface turbulent fluxes for a mountain glacier in the Cariboo Mountains, BC, Canada, The Cryosphere, 11, 2897-2918, doi: 10.5194/tc-11-2897-2017, 2017.

Ritter, F., Steen-Larsen, H. C., Werner, M., Masson-Delmotte, V., Orsi, A., Behrens, M., et al.: Isotopic exchange on the diurnal scale between near-surface snow and lower atmospheric water vapor at Kohnen station, East Antarctica, The Cryosphere, 10(4), 1647-1663, doi: 10.5194/tc-10-1647-2016, 2016.

Sokratov, S. A., & Golubev, V. N.: Snow isotopic content change by sublimation, Journal of Glaciology, 55(193), 823-828, doi: 10.3189/002214309790152456, 2009.

Steen-Larsen, H. C., Johnsen, S. J., Masson-Delmotte, V., Stenni, B., Risi, C., Sodemann, H., et al. (2013). Continuous monitoring of summer surface water vapor isotopic composition above the Greenland Ice Sheet. Atmospheric Chemistry and Physics, 13(9), 4815-4828. https://doi.org/10.5194/acp-13-4815-2013.

Stenni, B., Scarchilli, C., Masson-Delmotte, V., Schlosser, E., Ciardini, V., Dreossi, G., et al. (2016), Three-year monitoring of stable isotopes of precipitation at Concordia Station, East Antarctica, The Cryosphere, 10(5), 2415-2428, doi: 10.5194/tc-10-2415-2016, 2016.

Stenni, B., Curran, M. A. J., Abram, N. J., Orsi, A., Goursaud, S., Masson-Delmotte, V., et al.: Antarctic climate variability on regional and continental scales over the last 2000 years, Climate of the Past, 13(11), 1609-1634. doi: 10.5194/cp-13-1609-2017, 2017.

Surma, J., Assonov, S., & Staubwasser, M.: Triple Oxygen Isotope Systematics in the Hydrologic Cycle, Reviews in Mineralogy and Geochemistry, 86(1), 401-428, doi: 10.2138/rmg.2021.86.12, 2021.

Touzeau, A., Landais, A., Morin, S., Arnaud, L., & Picard, G.: Numerical experiments on vapor diffusion in polar snow and firn and its impact on isotopes using the multi-layer energy balance model Crocus in SURFEX v8.0, Geoscientific Model Development, 11(6), 2393-2418, doi: 10.5194/gmd-11-2393-2018, 2018.

Touzeau, A., Landais, A., Stenni, B., Uemura, R., Fukui, K., Fujita, S. et al.: Acquisition of isotopic composition for surface snow in East Antarctica and the links to climatic parameters, The Cryosphere, 10(2), 837-852, doi: 10.5194/tc-10-837-2016, 2016.

Town, M. S., Warren, S. G., Walden, V. P., & Waddington E. D.: Effect of atmospheric water vapor on modification of stable isotopes in near-surface snow on ice sheets, Journal of Geophysical Research, 113, D24303, doi: 10.1029/2008JD009852, 2008.

Van Liefferinge, B., Pattyn, F., Cavitte, M. G. P., Karlsson, N. B., Young, D. A., Sutter, J., et al.: Promising Oldest Ice sites in East Antarctica based on thermodynamical modelling, The Cryosphere, 12(8), 2773-2787, doi: 10.5194/tc-12-2773-2018, 2018.

Vignon, E., Genthon, C., Barral, H., Amory, C., Picard, G., Gallée, H., et al.: Momentum- and Heat-Flux Parametrization at Dome C, Antarctica: A Sensitivity Study, Boundary-Layer Meteorology, 162(2), 341-367, doi: 10.1007/s10546-016-0192-3, 2017.

Wahl, S., Steen-Larsen, H. C., Reuder, J., & Hörhold, M.: Quantifying the Stable Water Isotopologue Exchange Between the Snow Surface and Lower Atmosphere by Direct Flux Measurements, Journal of Geophysical Research: Atmospheres, 126, e2020JD034400, doi: 10.1029/2020jd034400, 2021.

Wahl, S., Steen-Larsen, H. C., Hughes, G., Dietrich, L., Zuhr, A., Behrens, M., et al.: Atmosphere-Snow Exchange Explains Surface Snow Isotope Variability, Geophysical Research Letters, 49(20), e2022GL099529, doi: 10.1029/2022GL099529, 2022.

WAIS Divide project members: Onset of deglacial warming in West Antarctica driven by local orbital forcing, Nature, 500(7463), 440-444, doi: 10.1038/nature12376, 2013.

Wang, Y., Sodemann, H., Hou, S., Masson-Delmotte, V., Jouzel, J., & Pang, H.: Snow accumulation and its moisture origin over Dome Argus, Antarctica, Climate Dynamics, 40(3-4), 731-742, doi: 10.1007/s00382-012-1398-9, 2012.

Werner, M., Langebroek, P. M., Carlsen, T., Herold, M., & Lohmann, G.: Stable water isotopes in the ECHAM5 general circulation model: Toward high-resolution isotope modeling on a global scale, Journal of Geophysical Research: Atmosphere, 116, D15109, doi: 10.1029/2011jd015681, 2011.

Table 1: Key initial values for model simulations.

Site		Dome C	Dome A	Dome A
Period		Summer (5th-16th, January)	Summer (December-February)	Winter[c] (June-August)
H_0 (m)		10	15	15
h_0 (cm)		1.50	1.50	1.50
Snow isotopic composition (‰)	$\delta^{18}O_{s0}$	-51.1647.00	-48.18	-61.92
	δD_{s0}	-394.00370.00	-372.90	-474.72
	d-ex_{s0}	15.286.00	12.54	20.94
Water vapor isotopic Composition in the near-surface atmospheric layer (‰)	$\delta^{18}O_{v0}$	-68.00	-70.40[a]/-70.41[b]	-94.69
	δD_{v0}	-490.00	-500.59/-500.64	-625.54
	d-ex_{v0}	52.00	62.64/62.67	132.00
Water vapor isotopic composition in the advected air masses (‰)	$\delta^{18}O_{fl}$	-63.00	-63.00	-88.00
	δD_{fl}	-440.00	-440.00	-574.00
	d-ex_{fl}	64.00	64.00	130.00
ρ_s (kg·m^{-3})		350329	380	380

[a,b] Value corresponds to clear-sky condition and highly cloud condition, respectively; [c]Some of the winter conditions were set the same as in Summer (see details in Sections 2.2.3).

带格式表格
带格式的：上标
带格式的：上标
带格式表格
带格式的：字体: 倾斜
带格式的：字体: (中文) Times New Roman
带格式的：字体: 倾斜
带格式的：字体: (中文) Times New Roman
带格式的：字体: (中文) Times New Roman
带格式的：字体: 倾斜
带格式的：字体: 倾斜
带格式的：字体: (中文) +中文正文 (宋体), (中文) 中文(中国)
带格式的：下标
带格式的：上标

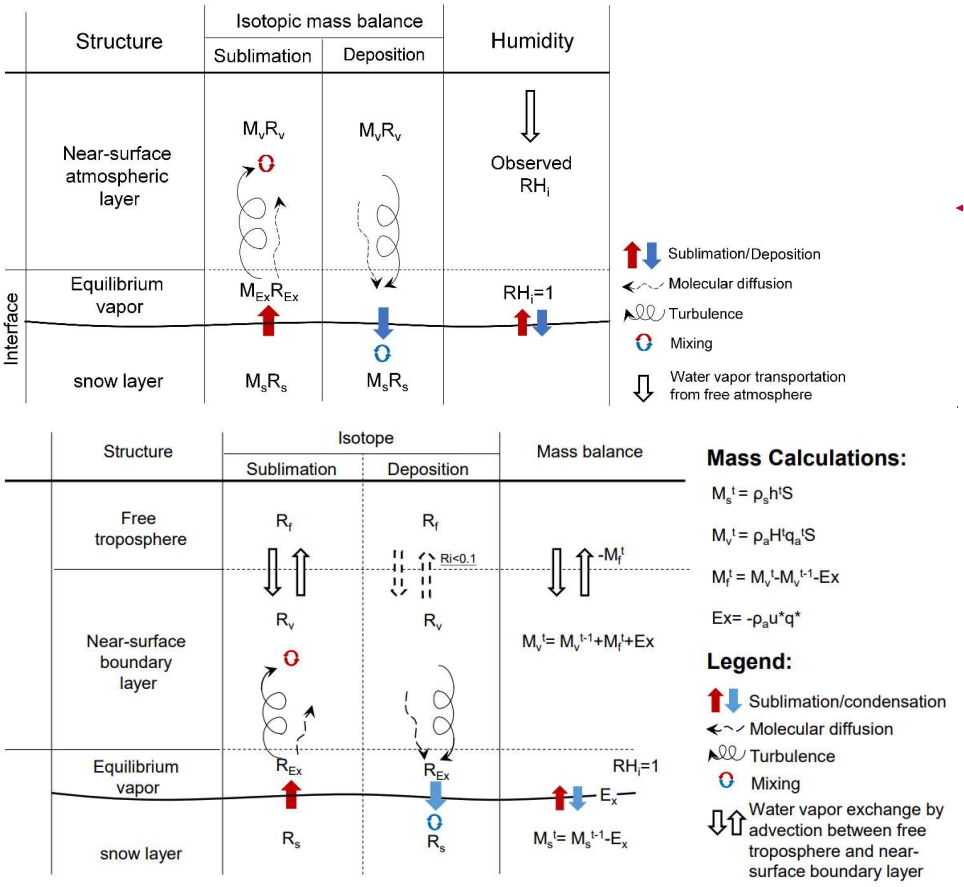

Figure 1: Schematic diagram of the box model used in this study.

775

带格式的：居中

带格式的：正文

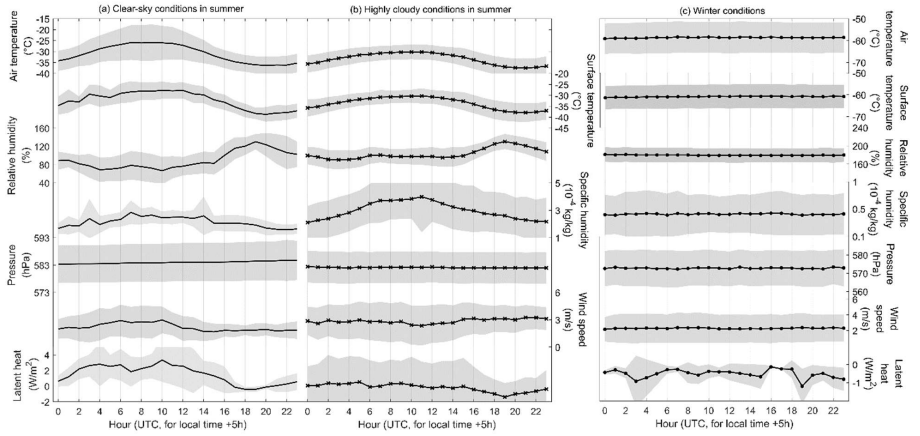

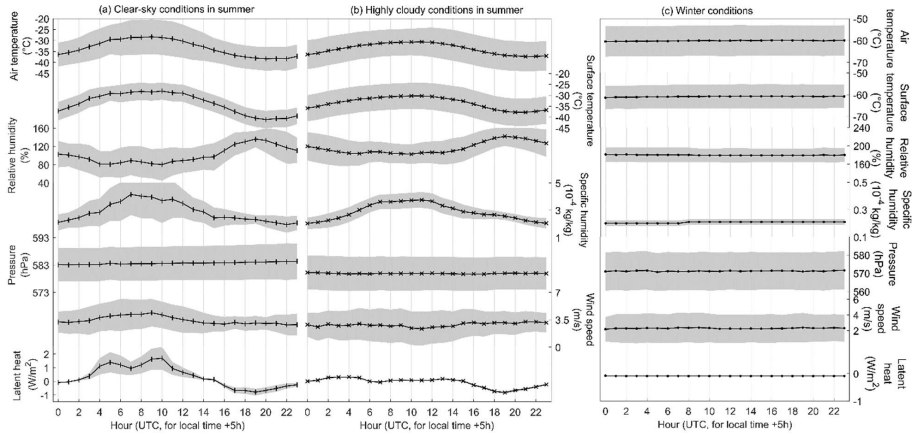

Figure 2: Stacks of diurnal cycles of meteorological parameters and the calculated latent heat under summer clear-sky conditions (a), summer highly cloudy conditions (b), and winter conditions (c) at Dome A. The hourly data for air temperature, relative humidity, air pressure and wind speed were averaged by AWS observations over those selected days. The diurnal variations for other three parameters were calculated based on hourly observations. In each panel, the solid line with marks represents the average

and the grey shadow is the standard deviation (±1σ). ~~The background color of pink and blue corresponds to the period dominated by sublimation and deposition, respectively, in a diurnal cycle.~~

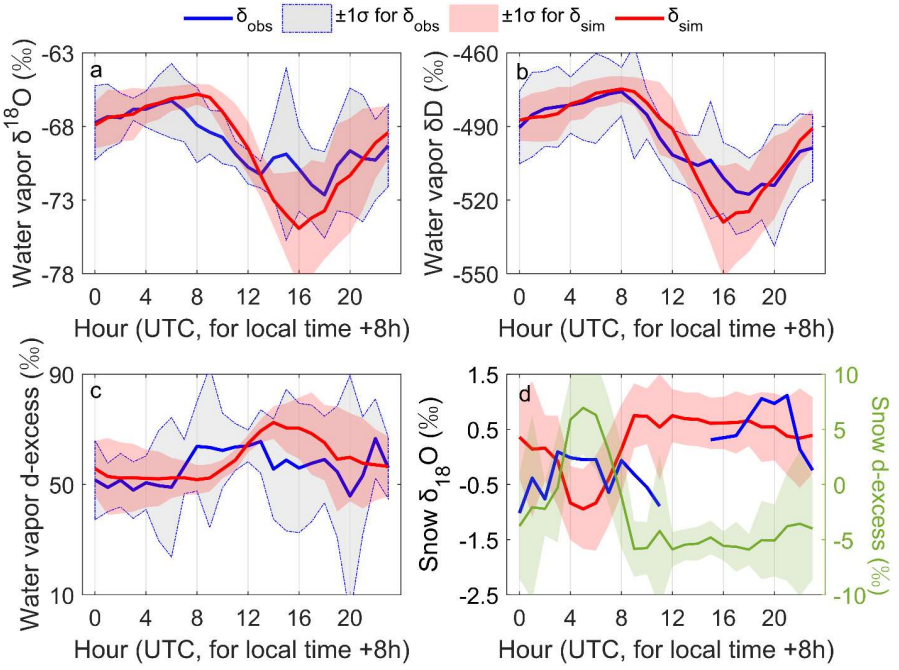

Figure 3: Model simulated diurnal variations of water vapor and snow isotopic compositions at Dome C along with the observations. (a) water vapor $\delta^{18}O$, (b) water vapor δD, (c) water vapor d-excess and (d) snow isotopes. In panels (a)-(c), blue solid line represents the observations of water vapor isotopic composition (δ_{obs}) with the light grey shaded area as the uncertainties (±1σ). The red solid line and the light red shaded area depicts the modelled variations of water vapor isotopic composition (δ_{sim}) and correspondingly uncertainties (±1σ). In panel (d), the modelled snow $\delta^{18}O$ and d-excess are shown as the blue solid line and green solid line, respectively. The red line represents the observed changes in snow $\delta^{18}O$ during Jan 6-7th, 2015. Note that their values are displayed with respect to the average value during the simulated period. The uncertainties in all four panels are also depicted with shaded areas like δ_{obs} and δ_{sim} in first three panels. The method for uncertainties estimation can be seen in SI (Texts S2).

带格式的: 字体: Times New Roman
带格式的: 字体: Times New Roman
带格式的: 居中
带格式的: 字体: 小五, 英语(英国)
带格式的: 非突出显示
带格式的: 字体: 小五, 英语(英国)
带格式的: 字体: 小五, 加粗, 英语(英国)
带格式的: 字体: 小五, 加粗
带格式的: 字体: 小五, 加粗, 英语(英国)
带格式的: 字体: 小五, 加粗
带格式的: 字体: 小五, 加粗, 英语(英国)
带格式的: 字体: 小五, 加粗
带格式的: 字体: 小五, 加粗, 英语(英国)
带格式的: 字体: 小五, 加粗
带格式的: 字体: 小五, 加粗, 英语(英国)
带格式的: 字体: 小五, 加粗
带格式的: 字体: 小五, 加粗, 英语(英国)
带格式的: 字体: 小五, 加粗, 英语(英国)
带格式的: 字体: 小五, 加粗
带格式的: 字体: 小五, 加粗, 英语(英国)
带格式的: 字体: 小五, 加粗
带格式的: 字体: 小五, 加粗, 英语(英国)
带格式的: 字体: 小五, 加粗, 英语(英国)
带格式的: 字体: 小五, 加粗
带格式的: 字体: 小五, 加粗, 英语(英国)
带格式的: 字体: 小五, 加粗, 英语(英国)
带格式的: 字体: 小五, 加粗, 英语(英国)
带格式的: 字体: 小五, 加粗
带格式的: 字体: 小五, 加粗
带格式的: 字体: 小五, 加粗
带格式的: 字体: 小五, 加粗, 英语(英国)
带格式的: 字体: 小五, 加粗
带格式的: 字体: 小五, 加粗
带格式的: 字体: 小五, 加粗, 英语(英国)

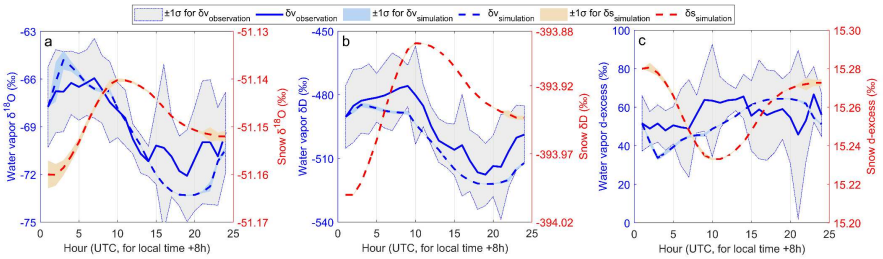

~~**Figure 3: Model simulated diurnal cycles of water vapor and snow isotopic compositions at Dome C along with the observations. (a) $\delta^{18}O$, (b) δD, and (c) d-excess. Blue solid line represents the observations of water vapor isotopic composition ($\delta v_{observation}$) with the light grey shaded area as the uncertainties (±1σ). The blue dotted line and the light blue shaded area depicts the modeled variations of water isotopic composition ($\delta v_{simulation}$) and correspondingly uncertainties (±1σ). The diurnal variations of modeled snow isotopic composition are shown as the red dotted line, and their uncertainties are close to those of $\delta v_{simulation}$. The method for uncertainties estimation can be seen in SI (Texts S2).**~~

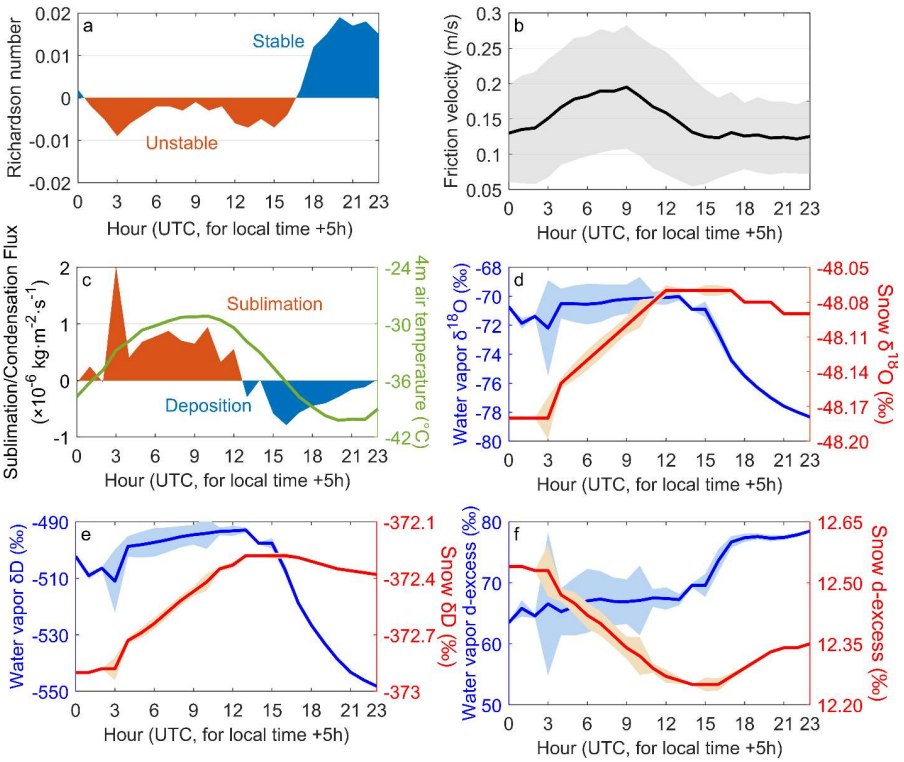
a
Stable
Unstable
Richardson number
0.02
0.01
0
-0.01
-0.02
0 3 6 9 12 15 18 21 23
Hour (UTC, for local time +5h)
b
Friction velocity (m/s)
0.3
0.25
0.2
0.15
0.1
0.05
0 3 6 9 12 15 18 21 23
Hour (UTC, for local time +5h)
c
Sublimation
Deposition
Sublimation/Condensation Flux
(×10^-6 kg·m^-2·s^-1)
2
1
0
-1
4m air temperature (°C)
-24
-30
-36
-42
0 3 6 9 12 15 18 21 23
Hour (UTC, for local time +5h)
d
Water vapor δ18O (‰)
-68
-70
-72
-74
-76
-78
-80
Snow δ18O (‰)
-48.05
-48.08
-48.11
-48.14
-48.17
-48.20
0 3 6 9 12 15 18 21 23
Hour (UTC, for local time +5h)
e
Water vapor δD (‰)
-490
-510
-530
-550
Snow δD (‰)
-372.1
-372.4
-372.7
-373
0 3 6 9 12 15 18 21 23
Hour (UTC, for local time +5h)
f
Water vapor d-excess (‰)
80
70
60
50
Snow d-excess (‰)
12.65
12.50
12.35
12.20
0 3 6 9 12 15 18 21 23
Hour (UTC, for local time +5h)

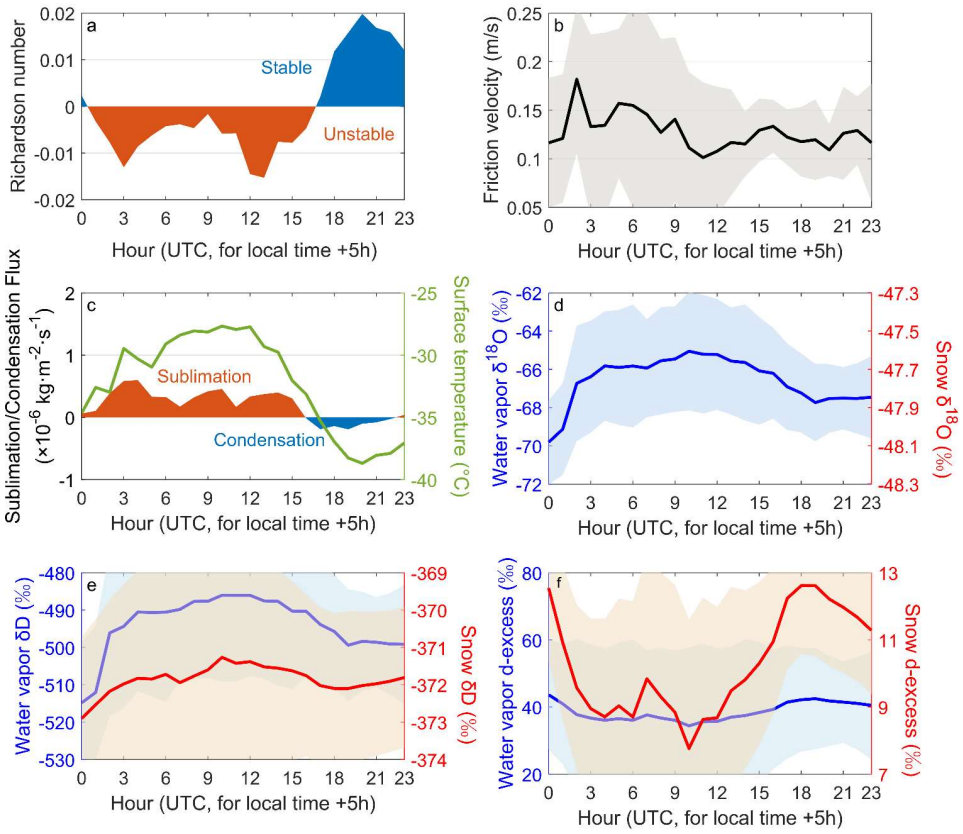

805

Figure 4: The simulated hourly mean vapor exchange flux and variations in atmospheric water vapor and snow isotopes under summer clear-sky conditions at Dome A: (a) Richardson number, (b) friction velocity, (c) vapor exchange flux, (d) snow and water vapor $\delta^{18}O$, (e) snow and water vapor δD, (f) snow and water vapor d-excess. The uncertainties for each variable are displayed by shaded area in each subpanel.

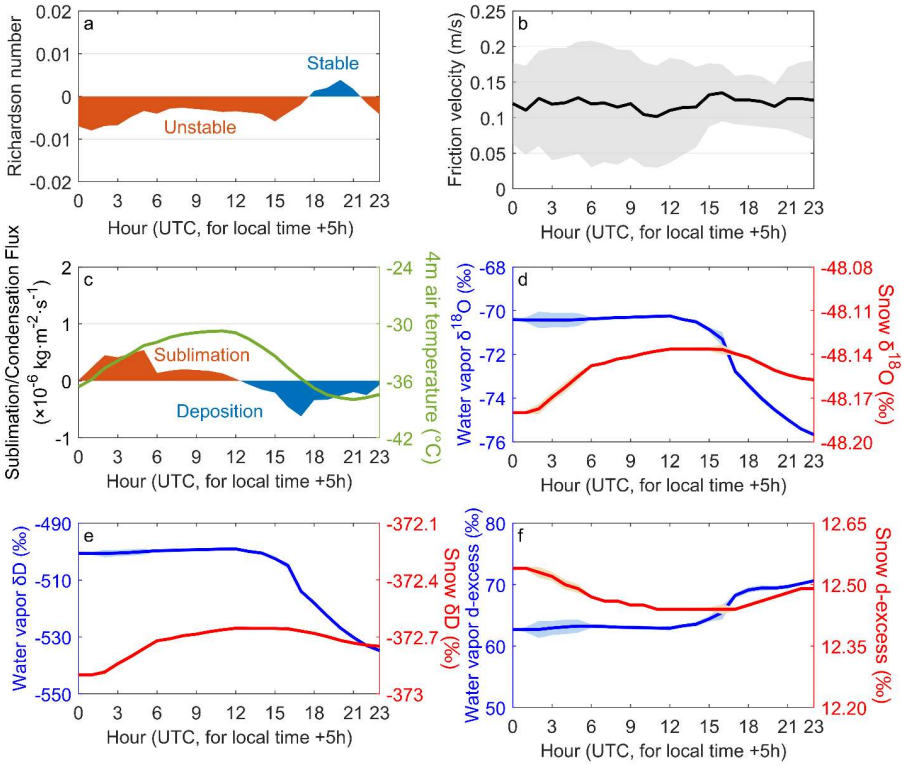
a
Richardson number
Stable
Unstable
Hour (UTC, for local time +5h)
b
Friction velocity (m/s)
Hour (UTC, for local time +5h)
c
Sublimation/Condensation Flux
(×10⁻⁶ kg·m⁻²·s⁻¹)
Sublimation
Deposition
4m air temperature (°C)
Hour (UTC, for local time +5h)
d
Water vapor δ18O (‰)
Snow δ18O (‰)
Hour (UTC, for local time +5h)
e
Water vapor δD (‰)
Snow δD (‰)
Hour (UTC, for local time +5h)
f
Water vapor d-excess (‰)
Snow d-excess (‰)
Hour (UTC, for local time +5h)

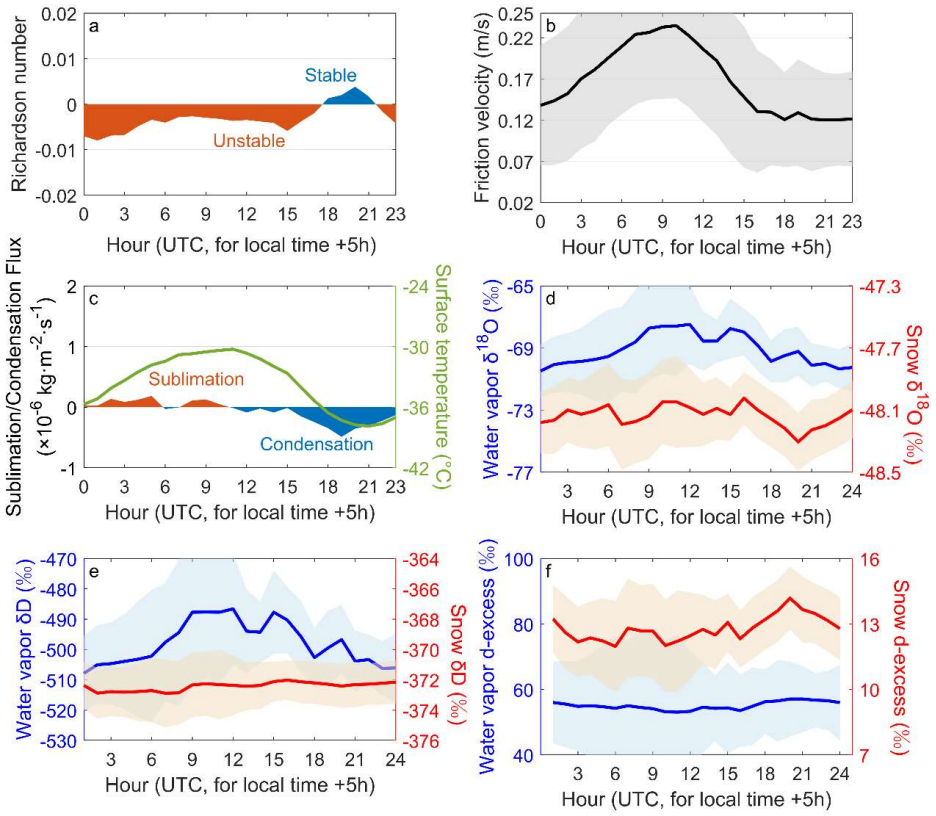

Figure 5: Same to Figure 4 but for Dome A under highly cloudy conditions in summer.

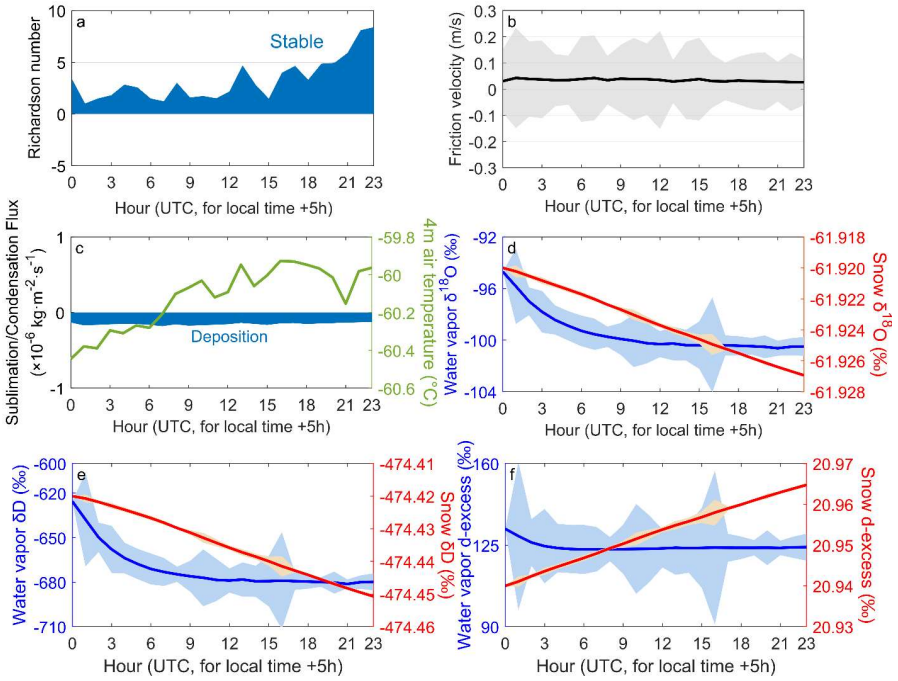
a
Stable
Richardson number
Hour (UTC, for local time +5h)
b
Friction velocity (m/s)
Hour (UTC, for local time +5h)
c
Deposition
Sublimation/Condensation Flux
(×10-6 kg·m-2·s-1)
4m air temperature (°C)
Hour (UTC, for local time +5h)
d
Water vapor δ18O (‰)
Snow δ18O (‰)
Hour (UTC, for local time +5h)
e
Water vapor δD (‰)
Snow δD (‰)
Hour (UTC, for local time +5h)
f
Water vapor d-excess (‰)
Snow d-excess (‰)
Hour (UTC, for local time +5h)

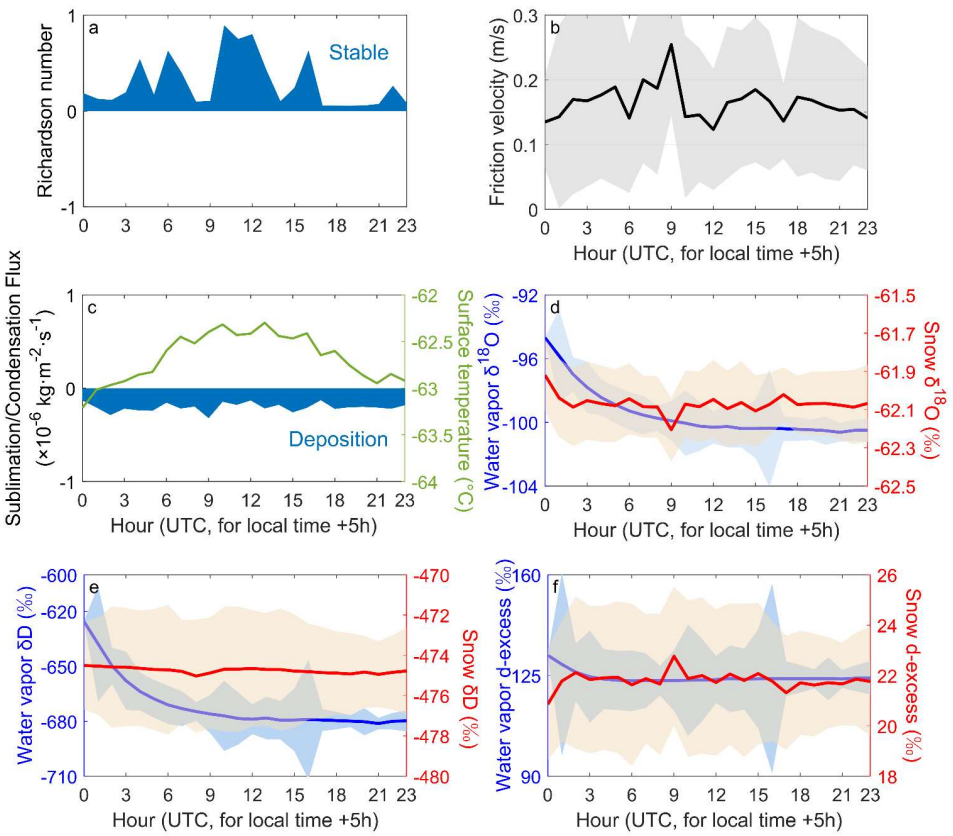

Figure 6: Same to Figure 4 but for Dome A under winter conditions.

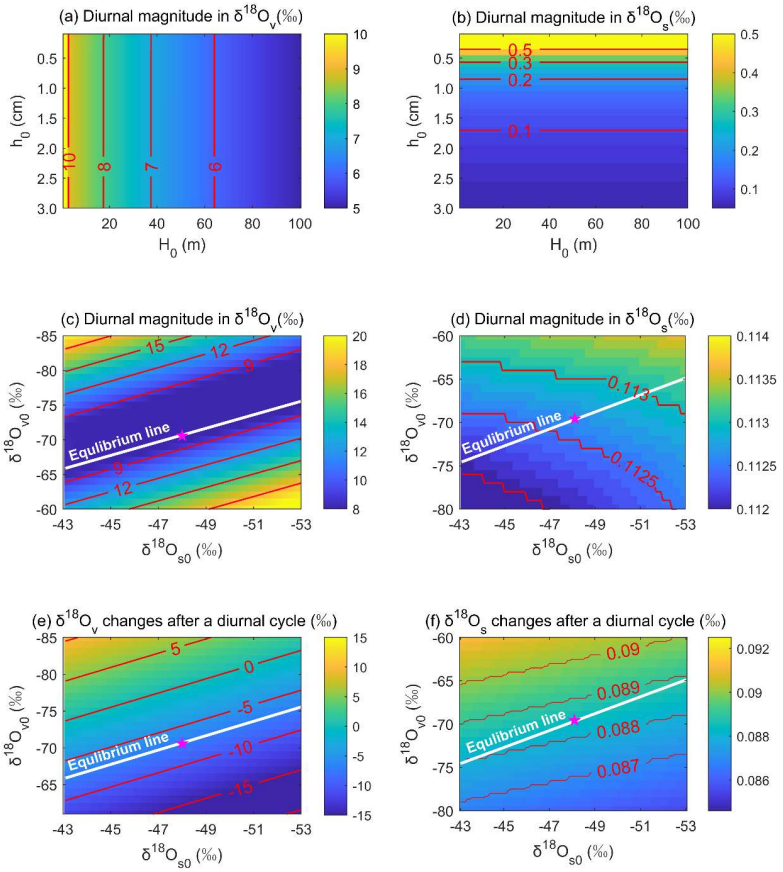
(a) Diurnal magnitude in δ18Ov(‰)
h0 (cm)
H0 (m)
10
8
7
6
(b) Diurnal magnitude in δ18Os(‰)
0.5
0.3
0.2
0.1
(c) Diurnal magnitude in δ18Ov(‰)
Equilibrium line
15
12
9
12
δ18Ov0 (‰)
δ18Os0 (‰)
(d) Diurnal magnitude in δ18Os(‰)
0.113
0.1125
(e) δ18Ov changes after a diurnal cycle (‰)
5
0
-5
-10
-15
(f) δ18Os changes after a diurnal cycle (‰)
0.09
0.089
0.088
0.087

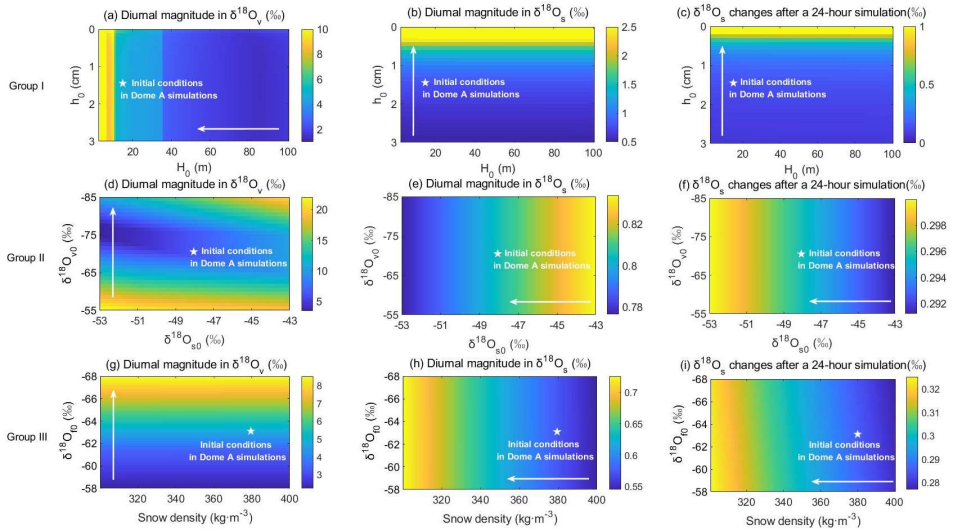

Figure 7: Sensitivity of the modelled results to changes in initial conditions. Panel 7a ~~and~~ ~~Panel~~ 7cb displays the modelled magnitudes ~~of~~ of $\delta^{18}O$ diurnal ~~cycle~~ variations in water vapor ($\delta^{18}O_v$), the modelled magnitude of $\delta^{18}O$ diurnal variations in ~~and~~ surface snow ($\delta^{18}O_s$), and $\delta^{18}O_s$ differences between the ending and starting values varying with different surface snow thickness (h_0) and boundary layer height (H_0). Panel 7dc-7f ~~and Panel 7d~~ shows the sensitivity of simulated results ~~of modeled $\delta^{18}O_v$ and $\delta^{18}O_s$ magnitudes~~ to changes in initial water vapor ($\delta^{18}O_{v0}$) and surface snow isotopic composition ($\delta^{18}O_{s0}$), respectively. Panel 7ge ~~and~~ 7if is the same as ~~7e and 6~~d-7f, but ~~in a form of the 24-h difference between the ending and starting values~~testing the sensitivity to changes in advected water vapor isotopic composition ($\delta^{18}O_m$) and snow density (ρ_s). In each subpanel, white ~~line~~ star indicates the initial conditions used in Dome A simulations with clear-sky conditions~~equilibrium line between snow and vapor isotopes at the temperature of starting time~~. ~~Pink star~~White arrows corresponds to the direction of simulated results with the higher sensitivity ~~initial isotopic values used in diurnal simulations at Dome A~~.

带格式的：上标
带格式的：下标
带格式的：字体: (默认) +西文正文 (Times New Roman)
带格式的：字体: Times New Roman, 下标
带格式的：英语(美国)